Precambrian Research 294 (2017) 91–110

Contents lists available at ScienceDirect

Precambrian Research

journal homepage: www.elsevier.com/locate/precamres

Neoproterozoic post-collisional extension of the central Jiangnan Orogen: Geochemical, geochronological, and Lu-Hf isotopic constraints from the ca. 820–800 Ma magmatic rocks

Yujia Xin [a,b], Jianhua Li [a,*], Shuwen Dong [c], Yueqiao Zhang [c], Wenbao Wang [a], Hanshen Sun [a]

[a] Institute of Geomechanics, Chinese Academy of Geological Sciences, Beijing 100081, China
[b] School of Earth and Space Sciences, Peking University, Beijing 100871, China
[c] School of Earth Sciences and Engineering, Nanjing University, Nanjing, China

A R T I C L E I N F O

Article history:
Received 19 December 2016
Revised 10 March 2017
Accepted 15 March 2017
Available online 18 March 2017

Keywords:
Neoproterozoic
South China
U-Pb zircon ages
Hf isotopes
S-type granitoids
Post-collisional extension

A B S T R A C T

Neoproterozoic magmatic rocks in South China contain important information on evaluating crustal reworking during the Yangtze-Cathaysia collision and post-collisional extension. We present here geochemical, geochronological, and Lu-Hf isotopic data of a suite of granitoids and diorites from the Jiuling and Meixian plutons of the central Jiangnan Orogen. The granitoids display intermediate geochemical features between S-type and I-type granites. They exhibit arc-like patterns of REE and trace element partition, reflecting inheritance of juvenile arc-derived crust. Igneous zircons from the Jiuling and Meixian granitoids yield U-Pb ages of 822–819 Ma and 816–815 Ma, respectively. Inherited zircons from the granitoids commonly yield a major age population of 980–860 Ma, consistent with the time of the Shuangxiwu volcanic arc. The igneous and inherited zircons have highly variable $\varepsilon_{Hf}(t)$ values ranging from −9 to +12.2. We interpret the granitoids to have been generated by remelting and binary mixing of (1) juvenile arc-derived crustal material and (2) supracrustal material of the Shuangqiaoshan metasedimentary rocks. The previous crustal thickening achieved by the Yangtze-Cathaysia collision is a prerequisite for their generation. The two granitoids, together with regional 825–815 Ma S-type granites, indicate incipient post-collisional collapse of thickened crust, heralding tectonic switch from compression to extension. The Meixian diorites display arc-like geochemical characteristics, and yield zircon U-Pb ages of 805–804 Ma and neutral to positive zircon $\varepsilon_{Hf}(t)$ values (−0.1–+7.5). The diorites were generated by decompression melting of arc-derived lower crust, associated with asthenospheric mantle upwelling during continental rifting. Such rifting may be part of global Neoproterozoic rifting events that finally led to breakup of the Rodinia supercontinent.

1. Introduction

South China, as one of the most important terranes of Southeast Asia, was formed through Neoproterozoic amalgamation of the Yangtze and Cathaysia blocks (Fig. 1) (Li et al., 2002a, 2007, 2009; Zhao and Cawood, 1999, 2012). How the two blocks amalgamated is an important issue that has potential significance in understanding the accretion of Southeast Asia, as well as on the assembly and configuration of the supercontinent Rodinia. Focusing on this issue, a series of studies have been conducted since 1990s, and they provide robust evidence that reveals the time and petrogenesis of arc magmas, blueschists, ophiolites and granitoids, all important in understanding the oceanic subduction, closure and arc-continent collision during the amalgamation (e.g., Shu et al., 1993; Charvet et al., 1996; Shu and Charvet, 1996; Li et al., 2003a, 2008, 2009; Wu et al., 2006; Wang et al., 2007a, 2008a,b, 2013a, 2014a, 2015; Zhou et al., 2009).

Mid-Neoproterozoic magmatic rocks, mostly formed at 830–740 Ma, are widespread across South China (Li et al., 1999, 2003a; Zheng et al., 2008; Zhou et al., 2009; Zhao et al., 2008, 2011; Wang et al., 2012a, 2013b, 2014b; Yao et al., 2012, 2014a, b). These rocks contain reliable information on evaluating crustal reworking and growth during the Yangtze-Cathaysia collision and post-collisional extension, as well as on the assembly and breakup of the supercontinent Rodinia. To interpret the origin of the magmatic rocks, three competing tectonic models have been proposed, i.e., the plume-rift, slab-arc, and plate-rift models (Li et al., 1999, 2003a; Zhou et al., 2002a; Zheng et al., 2008). The plume-rift model relates the mid-Neoproterozoic magmatism to

* Corresponding author.
E-mail address: lijianhua0301@126.com (J. Li).

http://dx.doi.org/10.1016/j.precamres.2017.03.018

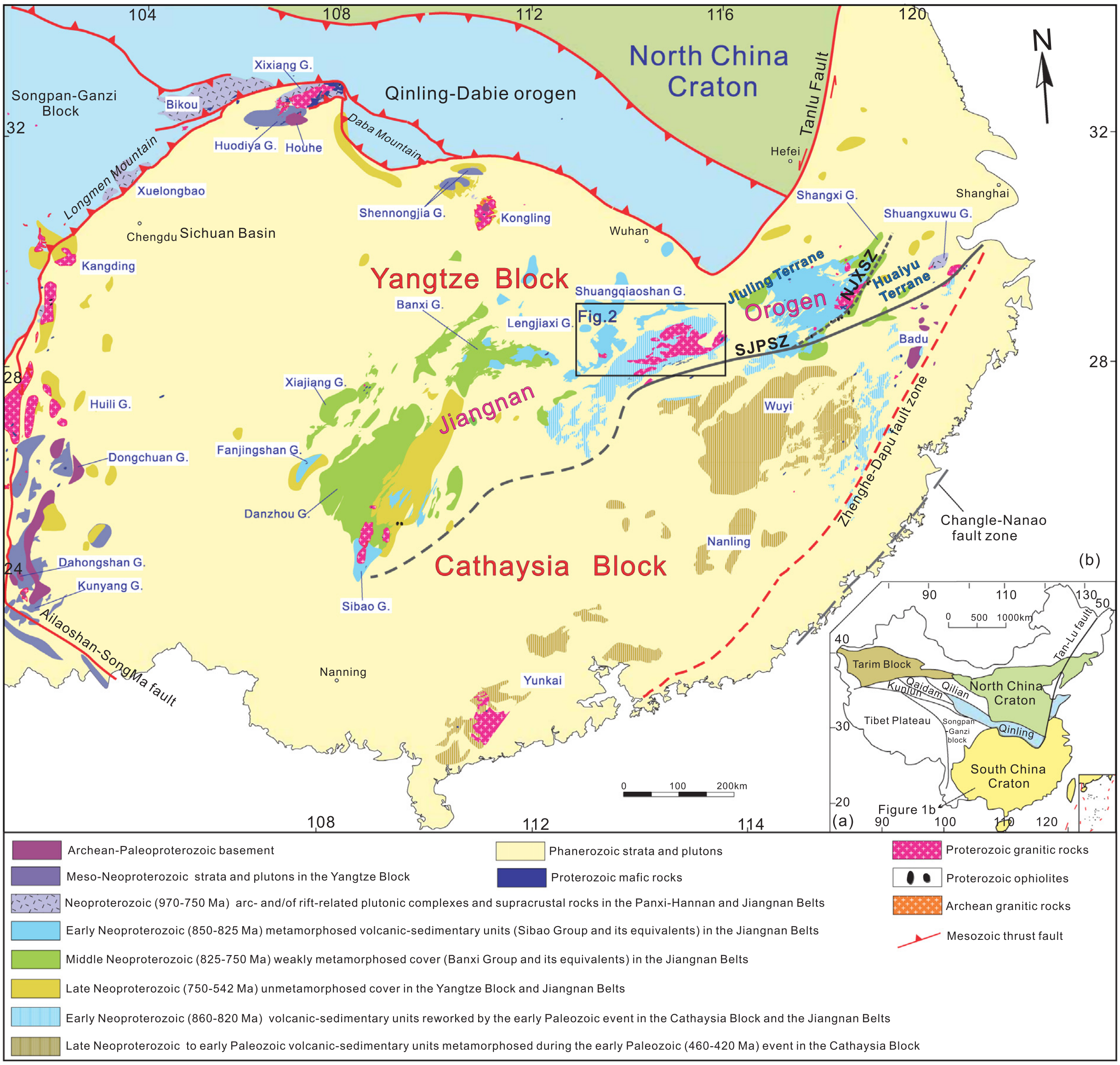

Fig. 1. (a) Sketch map showing the location of South China, modified after Li et al. (2016a). (b) Simplified geological map of South China showing the distributions of major Precambrian basements and igneous rocks, modified after Zhao and Cawood (2012). SJPSZ, Shaoxing-Jiangshan-Pingxiang suture zone. NJXSZ, Northeastern Jiangxi suture zone.

mantle plume activity that led to the breakup of Rodinia (Li et al., 1999, 2002b, 2003a,b, 2005). The slab-arc model interprets the magmatism to have occurred at an active continental margin, associated with eastward (present-day orientation) subduction of oceanic lithosphere beneath the western margin of the Yangtze Block (Zhou et al., 2002a,b; Zhou et al., 2006a,b; Zhao and Zhou, 2007a,b). The plate-rift model attributes the magmatism to reworking of the juvenile crust in response to post-collisional collapse and lithospheric extension (Zheng et al., 2007, 2008). The three models assume different locations of South China in Rodinia: the plume-rift model locates South China at a central position in Rodinia, sitting between Australia and Laurentia (Li et al., 1995, 1999), whereas the slab-arc and plate-rift models interpret South China to either be on the periphery of Rodinia (Zheng et al., 2008; Zhou et al., 2006a), or be an isolated continent unrelated to the supercontinent (Zhou et al., 2002a).

The Jiuling and Meixian plutons, located in the central part of the Jiangnan Orogen (Figs. 1 and 2a), hold the key to addressing the above controversies. Previous U-Pb dating of igneous zircons from the Jiuling granitoids yielded ages of 828–807 Ma (Li et al., 2003a; Wang et al., 2013b; Zhao et al., 2013; Zhong et al., 2005). The petrogenesis and tectonic implications of the granitoids continue to be hotly debated. Li et al. (2003a) interpreted the granitoids as resulting from crustal anatexis caused by conductive heating above a mantle plume, whereas Wang et al. (2004a) argued that the granitoids were formed associated with post-collisional crustal melting, induced by upwelling of hot asthenosphere following slab breakoff. Yao et al. (2014b) interpreted the granitoids as collision-related products formed in response to the Yangtze-Cathaysia collision. Alternatively, Zhao (2015) related the granitoids to partial melting of accretionary-wedge strata induced by underplating of mantle magmas, due to the oceanic lithospheric delamination. In contrast to the extensively studied igneous zircons within the Jiuling granitoids, few studies were conducted in the inherited zircons therein. In general, inherited zircons are interpreted as evidence that the host magma reached zircon saturation during melting (Harrison et al., 2007), and they are efficient at clarifying the magma source and petrogenesis of the granitoid.

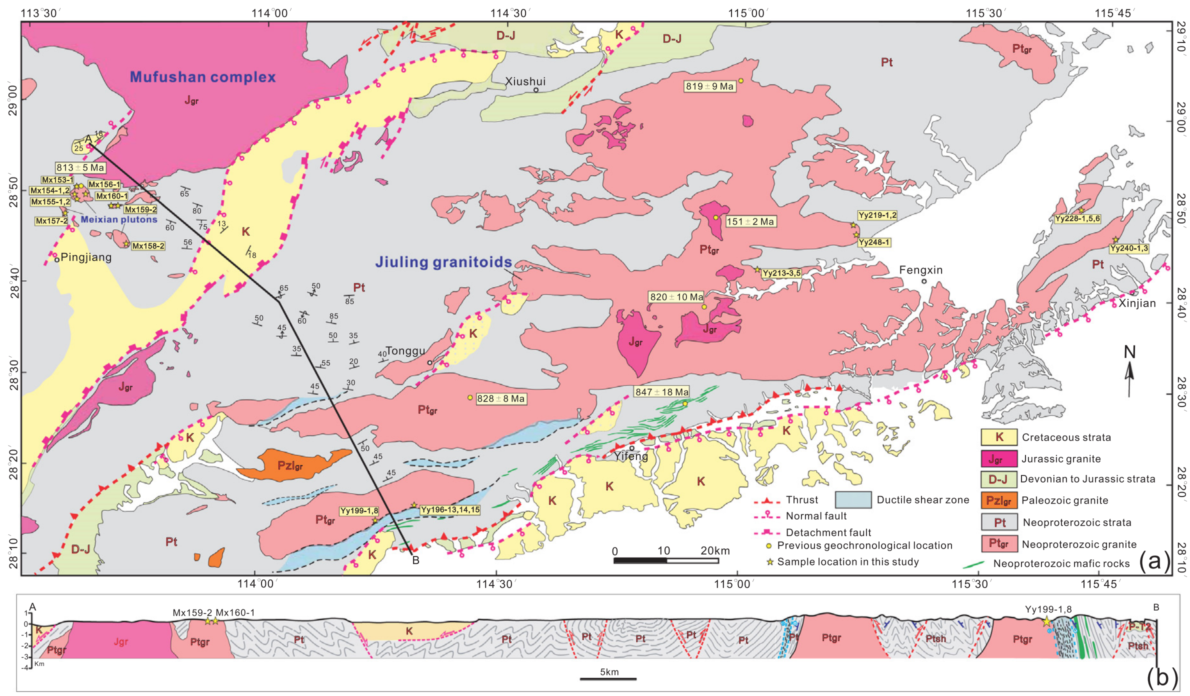

Fig. 2. (a) Geological map of the central Jiangnan Orogen, showing the distributions of the Jiuling and Meixian plutons, modified after Li et al. (2016c). See Fig. 1b for location; (b) Cross section A-B showing structural style of the central Jiangnan Orogen.

Therefore, in this study, we will determine the ages of inherited zircons from the Jiuling granitoids, and discuss their significance in the context of regional tectonic evolution. The Meixian plutons are located ~50 km to the west of the Jiuling granitoids. Previous study interpreted the Meixian plutons to have been emplaced in the Jurassic (Shi et al., 2013), coevally with the 154–146 Ma intermediate to felsic magmatism that generated the Mufushan complex (Wang et al., 2014c). However, recent work by Zhao et al. (2013) obtained one zircon U-Pb age of 813 ± 5 Ma for a granitoid sample. Due to the lack of time and geochemical constraints, the age, petrogenesis, and tectonic significance of the Meixian plutons remain poorly understood.

This paper presents combined results of new zircon U-Pb, whole-rock elements and Hf isotopes for the Jiuling and Meixian plutons. The results, together with previous data, constrain the emplacement time of the plutons to between 822 and 805 Ma, and support interpretation of the plutons as post-collisional extension-related magmatic rocks. These results shed new insights into Neoproterozoic crustal reworking in response to post-collisional extension in South China.

2. General geology of the Jiangnan Orogen

2.1. Proterozoic stratigraphic sequences

The Jiangnan Orogen, as an east-north-east trending orogenic collage extending for >1000 km across central South China (Fig. 1), was developed by Neoproterozoic oceanic subduction, closure, and collision/amalgamation of a variety of terranes between the Yangtze and Cathaysia Blocks (Wang et al., 2007a, 2013c, 2014a; Zhao, 2015). Much of the orogen is composed of Meso- and Neo-Proterozoic volcano-sedimentary units that record Neo-Proterozoic Yangtze-Cathaysia assembly (Wang et al., 2007a, 2008a) and Phanerozoic polyphase deformation (Chu and Li, 2014; Li et al., 2013, 2014, 2016a). The Mesoproterozoic volcano-sedimentary unit, termed the Tieshajie group, is mainly composed of greenschist facies gneisses, schists, slates and siltstones, interbedded by ~1.1 Ga bimodal assemblages of alkaline basalts and rhyolites (Gao et al., 2013a; Li et al., 2013a; Zhang et al., 2015a). This group was deposited in a Mesoproterozoic continental rift setting at a passive continental margin (Li et al., 2013a; Zhang et al., 2015a). The Neoproterozoic volcano-sedimentary units include the Shuangxiwu Group in west Zhejiang, the Shuangqiaoshan and Luokedong Groups in northwest Jiangxi, the Shangxi and Likou Groups in south Anhui, the Sibao and Danzhou Groups in north Guangxi, the Fanjingshan and Xiajiang Groups in northeast Guizhou, and the Lengjiaxi and Banxi Groups in central Hunan (Fig. 1b). The Shuangxiwu Group consists of typical arc rock assemblages with ages ranging from 970 to 850 Ma (Li et al., 2009; Gao et al., 2014a). The Shuangqiaoshan and Shangxi Groups were formed in the period 880–820 Ma; they are composed of spilite, keratophyre, tuff, metasandstone, phyllite and slate (Gao et al., 2008; Wang et al., 2008a, 2013c; Zhou et al., 2012; Li et al., 2016b). The Sibao, Fanjingshan and Lengjiaxi Groups, formed in the period 860–820 Ma, consist of greenschist-faces metamorphosed sandstone, siltstone and shale with minor tuff (bentonite), spilite, keratophyre, komatiitic rock and mafic–ultramafic sills (Wang et al., 2007a, 2010a, 2012b; Zhou et al., 2009; Li et al., 2011, 2013b; Yang et al., 2015). The Banxi and Danzhou Groups comprise slate, conglomerate, sandstone, meta-pelite and volcano-clastic rocks, and recent U-Pb zircon studies yield 820–750 Ma for the depositional time of these groups (Zhang et al., 2008a,b; Gao et al., 2010, 2013b; Wang et al., 2010a; Wang and Zhou, 2012). Based on contrasting structural styles, these volcano-sedimentary units are clarified into two rock sequences that are separated by a regional angular unconformity (Wang et al., 2007a; Zhao and Cawood, 2012). Rock sequences (>820 Ma) below the unconformity exhibit tight, isoclinal folds with penetrative cleavages, whereas those (<820 Ma) above the unconformity are flat-lying and display open folds with rare cleavage development (Wang et al., 2007a, 2013c).

2.2. Neoproterozoic magmatism

Two (Northeast Jiangxi and South Anhui) ophiolite suites crop out at the eastern end of the Jiangnan Orogen (Fig. 1). The Northeast Jiangxi ophiolite suite is mainly composed of harzburgites, wehrlites, gabbros, blueschists, spilites and adakitic granites; dating by Sm-Nd isochron and SHRIMP zircon U-Pb methods gave ages of ~1.0–0.9 Ga for the ophiolite suite (Chen et al., 1991; Shu et al., 1993, 2006; Li et al., 1994, 2008; Li and Li, 2003; Gao et al., 2009; Wang et al., 2015; Zhang et al., 2015). This ophiolite suite represents remnants of ancient oceanic lithosphere, and assists in tracing the Northeastern Jiangxi suture zone (NJXSZ) that separates the oceanic Huaiyu terrane from the continental Jiuling terrane (Fig. 1) (Charvet et al., 1996; Shu and Charvet, 1996; Yao et al., 2014a). For the South Anhui ophiolite suite, U-Pb dating of zircons from the gabbros yielded ages of ~860–833 Ma that might date the opening of a back-arc basin (Ding et al., 2008; Yin et al., 2013; Cui et al., 2017). In the western Jiangnan Orogen, an imbricated forearc ophiolitic mélange, composed of gabbros, diabases, cherts and siliceous marbles, was recently recognized in the Longsheng area (Yao et al., 2016a). Within the ophiolitic mélange, zircon U-Pb dating of gabbros and diabases gave ages of 863–869 Ma, which were interpreted as dating northwestward subduction of an oceanic plate (Yao et al., 2016a).

The Late Neoproterozoic (860–830 Ma) mafic–ultramafic rocks are distributed in local areas of the Jiangnan Orogen; they are interpreted as recording either opening of a back-arc basin in the central Jiangnan Orogen (Zhang et al., 2012a, 2013; Li et al., 2016b), or subduction of the oceanic lithosphere in the western Jiangnan Orogen (Wang et al., 2004a, 2016; Zhou et al., 2004, 2009; Yao et al., 2014a,b; Yao et al., 2015; Zhang and Wang, 2016). Neoproterozoic granitic rocks range in age from 970 to 740 Ma and vary in composition from I-, S- to A- types. The I-type granitoids, dated at 913–905 Ma, crop out in the eastern Jiangnan Orogen; they exhibit a calc-alkaline affinity and represent arc magmatism formed in response to the subduction of the oceanic lithosphere (Ye et al., 2007). The S-type granitoids, with ages ranging from 830 to 800 Ma, are mainly exposed in the Jiuling, Sanfang, Bendong and Yuanbaoshan areas (Li et al., 2003a; Zhong et al., 2005; Wang et al., 2006a, 2013b, 2014b; Zhao et al., 2013; Yao et al., 2014b). The A-type granitoids, mostly formed at 800–770 Ma, are interpreted as extension-related magmas generated in a rifting setting, associated with upwelling of deep asthenospheric mantle (Zheng et al., 2008; Wang et al., 2010b; Yao et al., 2014a) and tectonic collapse of the collision-thickened orogen (Wang et al., 2012a).

2.3. Neoproterozoic low-grade metamorphism and interpretations of the Neoproterozoic orogeny

Sharply different from granulite to eclogite facies metamorphism in typical continent-continent collisional belts (e.g., the Alpine, Himalayan and Dabie-Sulu belts; Hacker et al., 2000; Yin and Harrison, 2000; Schmid et al., 2004), all lithologies in the Jiangnan Orogen were only metamorphosed in sub-greenschist to greenschist facies (Shu et al., 1995; Shu and Charvet, 1996; Li et al., 2007; Wang et al., 2007a). The absence of syn-orogenic high-grade metamorphic rocks implies that there was either no deep continental subduction or no significant erosion/exhumation occurring during the orogeny (Zhao and Cawood, 2012).

To address the origin of the orogeny, Wang et al. (2007a, 2012a, 2014b) proposed a continent-arc-continent accretionary model that assumed the orogeny as resulting from the collision of the Shuangxiwu arc with the Yangtze and Cathaysia continents, whereas Wang et al. (2013a, 2014a) attributed the orogeny to sequential development and closure of the Wuyi-yunkai, Shuangxiwu, and Jiangnan arc-back-arc systems. Alternatively, Zhao (2015) interpret the orogeny as being developed by divergent double subduction along both sides of a single oceanic plate and soft collision of the Yangtze and Cathaysia blocks, without involving deep continental subduction as both continental blocks occupied upper plate positions.

3. Petrology and sampling

The Jiuling granitoids occur as a batholith that covers an outcrop area of ~2500 km^2 in the central Jiangnan Orogen. The granitoids are mainly composed of cordierite-bearing granodiorites and contain numerous mafic enclaves (Fig. 3a). In thin sections, the granodiorite comprises ~30% quartz, ~10–40% feldspars, ~20–40% plagioclase, ~10% biotite, ~5% cordierite, ~2% hornblende, and variable amounts of secondary muscovite (Fig. 3b). The country rocks are Neoproterozoic (~880–820 Ma) flysch turbidites of the Shuangqiaoshan Group (Charvet et al., 1996; Shu and Charvet, 1996). The contact between the Jiuling granitoids and the Shuangqiaoshan Group is characterized by heterogeneous rheology and ductile deformation, and forms arrays of E-trending high-strain ductile shear zones (Fig. 2a). Within the shear zones, the granodiorites are attenuated (Fig. 3c), forming an ~E-trending mylonitic foliation defined by the alignment of mica and quartz bands, and a gently plunging stretching lineation defined by stretched quartz grains and aligned mica clusters. Kinematic criteria, including σ-type plagioclase porphyroclasts flanked by elongated quartz wings (Fig. 3c), mica fishes and S-C fabrics (Fig. 3d), attest to a dextral shear motion. Recent studies indicate that the dextral shear occurred at ca. 460–420 Ma under greenschist-facies conditions, related to the intra-continental Yangtze-Cathaysia convergence (Chu and Lin, 2014; Li et al., 2016c). In this study, total 15 granodiorite and granite samples were collected from the Jiuling granitoids, for geochemical, zircon U-Pb and in-situ Hf isotopic analysis. The sample localities are shown in Fig. 2a.

The Meixian plutons, with an outcrop area of ~40 km^2, are located in the southernmost part of the Mufushan complex (Fig. 2a). The plutons consist predominantly of biotite plagioclase granite, granodiorite, and diorite. The biotite plagioclase granite is composed of ~55–73% plagioclase, ~18–30% quartz, ~3–11% biotite, and ~0–11% hornblende (Fig. 3e). The diorite is composed of ~60–70% plagioclase, ~20–25% hornblende, <5% quartz, <5% biotite, secondary chlorite and muscovite, and minor Fe-Ti oxides (Fig. 3f). Total 10 plagioclase granite, granodiorite, and diorite samples are collected for geochemical, zircon U-Pb and in-situ Hf isotopic analysis. See Fig. 2a for sample localities.

4. Analytical methods

Rock samples were cut into small chips, soaked in 4N hydrochloric acid for one hour to remove secondary carbonate minerals, and then powdered. Major and trace elements were analyzed at the National Research Center for Geoanalysis of Beijing. Major elements were determined by X-ray fluorescence (XRF) (Rigaku-3080) with analytical errors less than 0.5%. Trace elements Zr, Nb, V, Cr, Sr, Ba, Zn, Ni, Rb and Y were analyzed using the Rigaku-2100 with analytical errors <3–5%. Other trace elements and rare earth elements (REE) were analyzed by an inductively coupled plasma mass spectrometry (ICP-MS) using a TJA PQ-ExCell system. About 25 mg bulk-rock powder was dissolved in a high pressure Teflon bomb using a HF+HNO_3 mixture, and heated

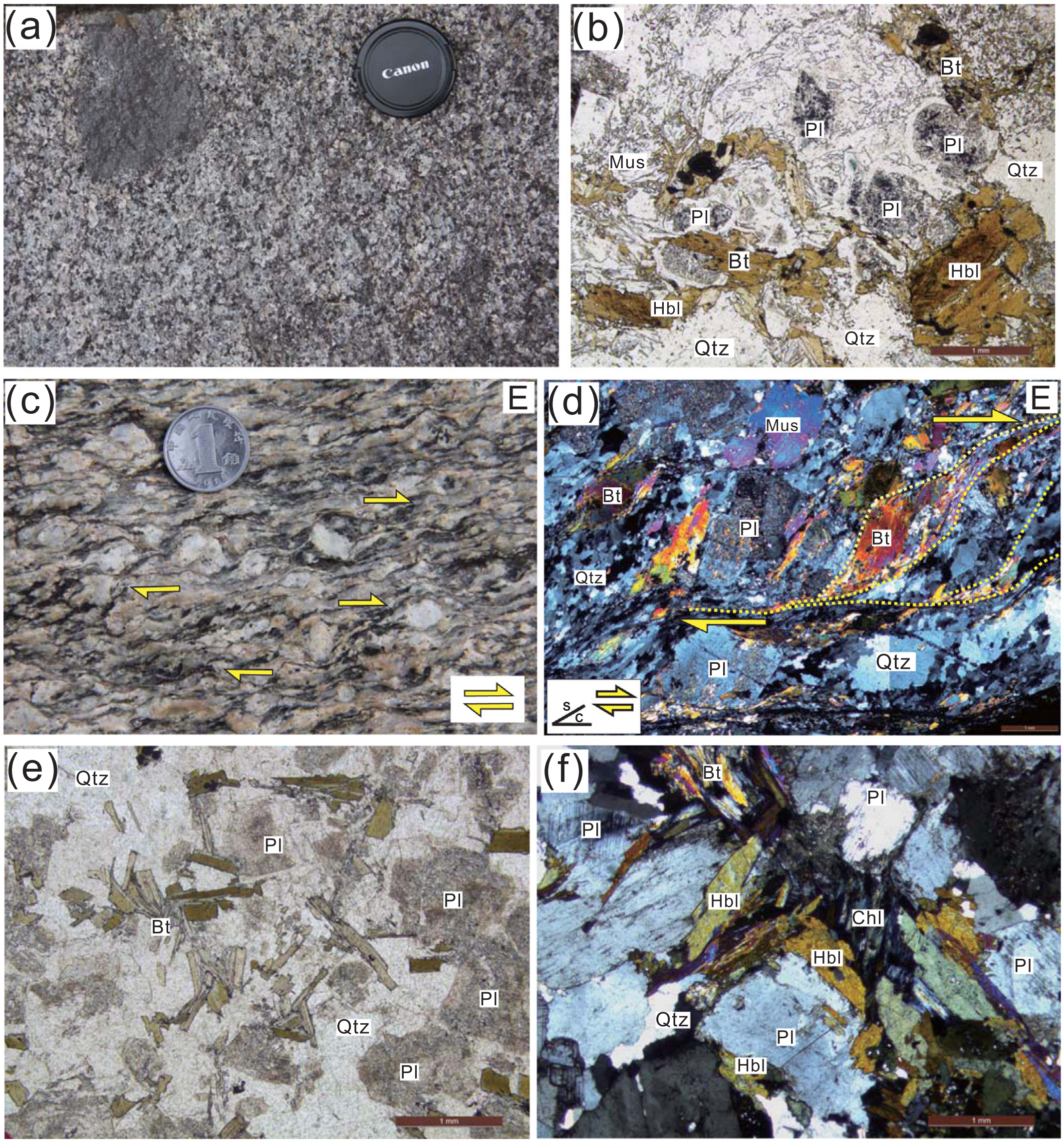

Fig. 3. Representative field photographs and photomicrographs of the Jiuling and Meixian plutons. (a) Field photograph of biotite granodiorite and mafic enclaves of the Jiuling granitoids (sample Yy240-1). (b) Micrograph photo of biotite granodiorite (sample Yy240-1) from the Jiuling plutons. It consists of quartz, plagioclase, biotite, hornblende and minor muscovite. (c) Field photograph of mylonitic granodiorite (sample Yy199-1). Asymmetrically elongated quartz tails around plagioclase porphyroclasts indicate dextral shear. (d) Asymmetric mica fishes and S-C fabrics consistently suggest a dextral shear sense (sample Yy196-13). (e) Mineral assemblages of plagioclase granite from the Meixian plutons: plagioclase + quartz + biotite (sample Mx160-1). (f) The diorite from the Meixian plutons consists of plagioclase, hornblende, and minor quartz, biotite, and chlorite (sample Mx154-1). Qtz, quartz; Pl, plagioclase; Bt, biotite; Mus, muscovite; Hbl, hornblende; Chl, chlorite.

to 190 °C for 48 h. Two international standards (GSR-1 and GSD-9) were chosen for calibration. The analytical discrepancy is <5% relative for elements with abundance >10 ppm, and 5–10% for those <10 ppm. Detailed analytical procedures are similar to those described by He et al. (2002).

Zircons for U-Pb dating were separated using conventional heavy liquid and magnetic techniques. The zircons were extracted, mounted in epoxy resin, and polished to about half thickness. Cathodoluminescence (CL) images were obtained using a JEOL scanning electron microscope, to reveal internal structures of the zircons. For samples from the Meixian pluton, in situ zircon U-Pb dating was conducted on the LA–ICP-MS at the State Key Laboratory of Geological Processes and Mineral Resources, China University of Geosciences, Wuhan. A pulsed 193-nm ArF Excimer laser, at a repetition rate of 10 Hz and an energy density of ~4 J/cm^2, was coupled to an Agilent 7500a ICP-MS instrument and used for ablation. The spot diameter and depth were 33 and 20 μm, respectively. Zircon 91,500 was used as an external standard to calibrate isotope fractionation. NIST SRM 612 was analyzed every 10 analyses to normalize U, Th and Pb concentrations of unknowns. Each analysis incorporated a background acquisition of ~20–30 s (gas blank), followed by 50 s data acquisition utilizing an Agilent Chemstation. Off-line selection and integration of background and analytical signals, time-drift correction, and quantitative calibration were performed using ICPMSDataCal (Liu et al., 2008, 2010a). More detailed operating conditions were described by Liu et al. (2008, 2010). For samples from the Jiuling granitoids, in situ zircon U–Pb dating was performed using a laser ablation (LA)-MC-ICP-MS, attached to a New Wave UP193FX ArF Excimer laser ablation system, at the Tianjin Institute of Geology and Mineral Resources. Laser sampling was conducted using a spot size of 35 μm, at a repetition rate of 8–10 Hz and an energy density of 7–8 J/cm^2. Two standard zircons (GJ-1 and 91500) were used to calibrate the U-Th-Pb ratios and absolute U abundance. The detailed analytical techniques and operating conditions have been described by Li et al. (2010). For all analyses, common Pb corrections were calculated using the method described by Andersen (2002). Age calculations and plotting of concordia diagrams were made using ISOPLOT (ver 3.0) (Ludwig, 2003). Uncertainties on the weighted mean ages were calculated at 1σ error.

In situ zircon Lu–Hf isotopic analysis was carried out at the Tianjin Institute of Geology and Mineral Resources for the Jiuling granitoids, and at the Nanjing FocuMS Technology Co. Ltd for the Meixian plutons. The two laboratories adopt the same instrument system, i.e., the Neptune MC-ICP-MS system equipped with a Geolas-193 laser-ablation system. Therefore, their operating conditions and analytical procedures are broadly consistent and briefly described as follows. The Hf analyses were made on the same zircon spots that were previously analyzed for U–Pb isotopes, with ablation pits of 50 μm in diameter and a repetition rate of 8 Hz. Standard zircons, including GJ-1, 91500, Mud Tank and Penglai, were analyzed to evaluate the accuracy of the laser-ablation results. The He and Ar carrier gases were used to transport the ablated sample from the laser ablation cell to the ICP-MS torch via a mixing chamber. The isobaric interference of ^{176}Lu and ^{176}Yb on ^{176}Hf is corrected using the ratios of $^{176}Lu/^{175}Lu = 0.02655$ and $^{176}Yb/^{172}Yb = 0.5887$ (Vervoort et al., 2004). Detailed analytical procedures have been described by Griffin et al. (2000, 2002). During our analyses, the measured $^{176}Hf/^{177}Hf$ ratios are 0.282007 ± 000009 (2σ, n = 11) and 0.282513 ± 000012 (2σ, n = 5) for standard GJ-1 and Mud Tank, respectively. To calculate $\varepsilon_{Hf}(t)$ values, we adopted the present-day chondritic values of $^{176}Hf/^{177}Hf = 0.282772$ and $^{176}Lu/^{177}Hf = 0.0332$ (Blichert-Toft and Albarède, 1997). A decay constant for ^{176}Lu of $1{\cdot}865 \times 10^{-11}$ a^{-1} was used during the $\varepsilon_{Hf}(t)$ calculation (Scherer et al., 2001). Two-stage model age (T_{DM2}), generally used for rocks that are melted from the crustal protoliths (Wu et al., 2007; Zheng et al., 2007), was calculated by projecting the initial zircon $^{176}Hf/^{177}Hf$ ratios to the depleted mantle model growth curve, assuming a $^{176}Lu/^{177}Hf$ ratio of 0.015 for the average continent crust (Griffin et al., 2002).

5. Results

5.1. Major and trace elements

5.1.1. The Jiuling granitoids

Fifteen samples from the Jiuling granitoids were analyzed for whole-rock major and trace element compositions (Fig. 2a). A combination of results from this study and previous work (Li et al., 2003a; Wang et al., 2004b) has been shown in Figs. 4–7. Our analytical results are listed in Appendix Table S1.The granitoid samples exhibit SiO_2 = 65.61–69.54 wt%, Al_2O_3 = 14.76–16.25 wt%, FeOt = 3.52–4.95 wt%, MgO = 1.12–1.98 wt%, CaO = 1.11–2.11 wt%, P_2O_5 = 0.11–0.16 wt%, TiO_2 + FeOt + MgO = 5.22–7.60 wt%, and $K_2O + Na_2O$ = 5.8–6.63 wt%, plotting predominantly in the subalkaline granodiorite field (Fig. 4a). In the Hacker diagrams (Fig. 5a–i), these samples exhibit negative correlations of Al_2O_3, MgO, CaO, FeOt, P_2O_5 and TiO_2 with respect to SiO_2, but insignificant correlations between SiO_2 and K_2O, Na_2O and MnO; they are rich in K_2O, all falling into the domain of high-K calc-alkaline (Fig. 5b). All samples are strongly peraluminous and have A/CNK ratios of 1.3–1.45 (Fig. 4b, Table S1), consistent with the occurrence of Al-rich minerals (e.g., cordierite and garnet) in the granitoids (Li et al., 2003a; Wang et al., 2013b). Most of the above-stated signatures indicate a typical S-type affinity (Chappell and White, 1974, 1992), similar to those of the S-type granodiorites from the Lachlan Fold Belt (Maas et al., 1997; Sylvester, 1998; Clemens, 2003; Villaros et al., 2009). In addition to the S-type affinity, the samples also share

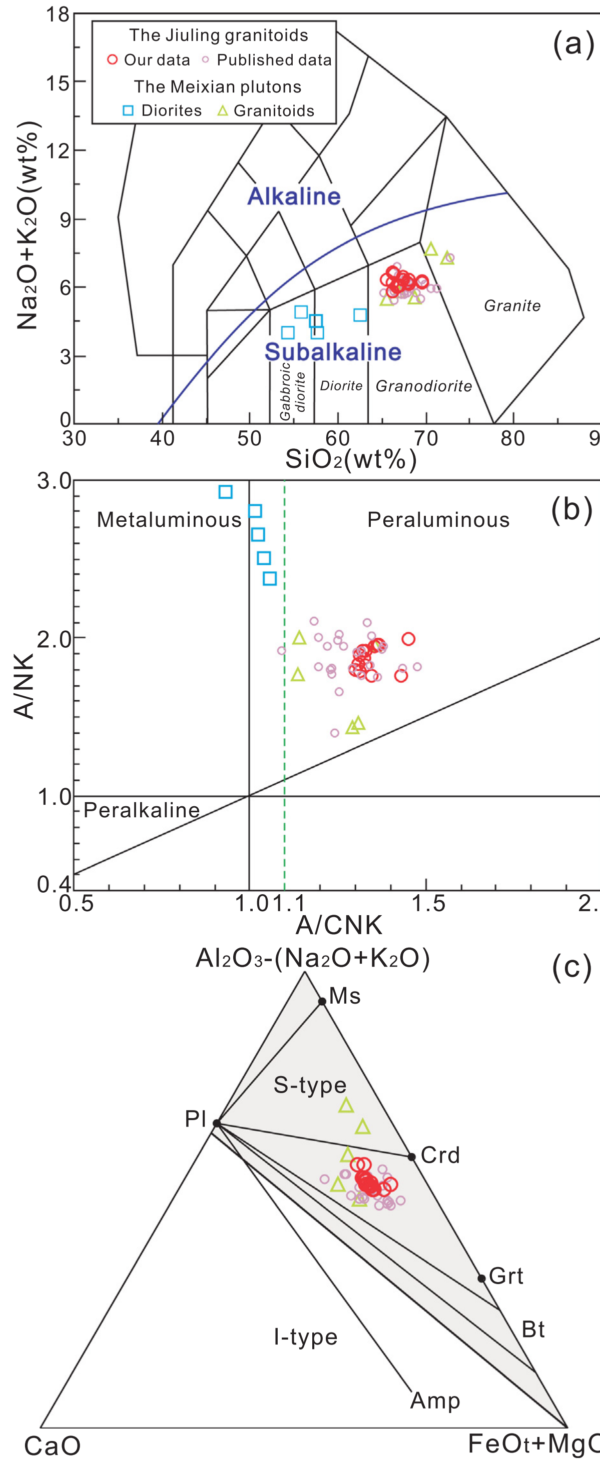

Fig. 4. (a) TAS diagram (after Middemost, 1994), (b) A/CNK vs. A/NK diagram (after Miniar and Piccoli, 1989) and (c) CaO-FeOt + MgO-Al_2O_3-($Na_2O + K_2O$) diagram (after White and Chappell, 1977) for the Jiuling and Meixian plutons. Published data for the Jiuling granitoids are from Li et al. (2003a) and Wang et al. (2004b). Symbols in Fig. 4b and c are the same as those in Fig. 4a.

some geochemical characteristics of I-type granites (Chappell and White, 1974, 1992), as expressed by negative correlation between P_2O_5 and SiO_2 (Fig. 5h) and extensive occurrence of hornblende (Fig. 3b). Chondrite-normalized REE patterns of the Jiuling granitoids are shown in Fig. 6a. Our samples have total REE contents of 119–189 ppm, and display variable enrichment in LREE with $(La/Yb)_N$ = 4.74–9.09 and minor HREE fractionation with (Gd/

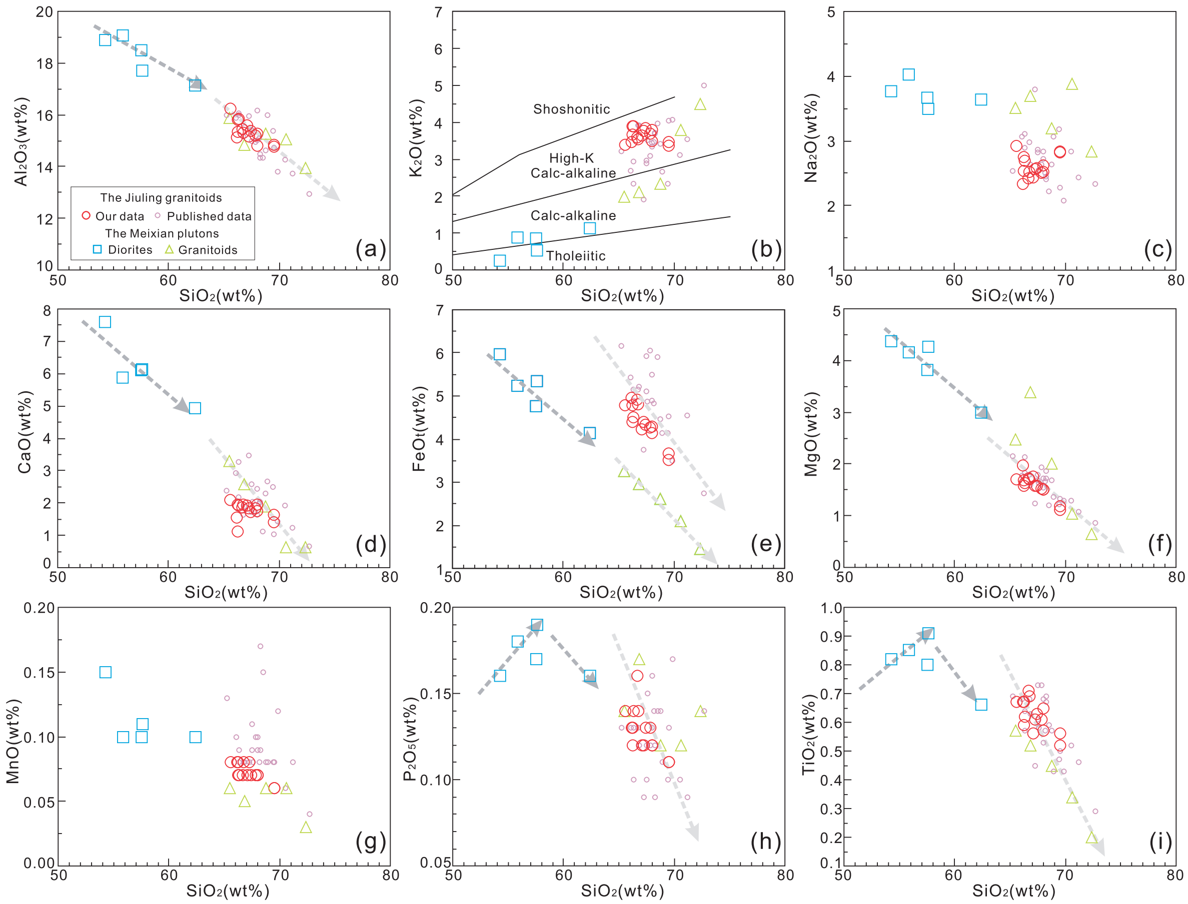

Fig. 5. SiO_2 versus (a) Al_2O_3; (b) K_2O; (c) Na_2O; (d) CaO; (e) FeOt; (f) MgO; (g) MnO; (h) P_2O_5; (i) TiO_2 for the Jiuling and Meixian plutons. Published data for the Jiuling granitoids (Li et al., 2003a; Wang et al., 2004b) are also indicated. Symbols in Fig. 5b–i are the same as those in Fig. 5a.

$Yb)_N$ = 1.33–1.96 (Table S1), consistent with previous results from Li et al. (2003a). They show prominently negative Eu anomalies with Eu/Eu* = 0.47–0.62, indicating plagioclase fractionation (Fig. 6a, Table S1). The fractionation of plagioclase is also supported by decreasing Sr with changeless Ba and negative correlation between Sr and Rb on the logarithmic plots of Sr versus Ba and Rb (Fig. 7a, b). On the primitive mantle-normalized spidergram, the samples exhibit enrichment in Rb, Th and U and significantly negative Ba, Nb, Sr, P and Ti anomalies (Fig. 6b), coinciding well with the character of crustally derived S-type magmas. The above-stated REE and trace element patterns are similar to those of Neoproterozoic (~820 Ma) and early Paleozoic (~460–420 Ma) peraluminous granites in the eastern Jiangnan Orogen and the Cathaysia block (Wu et al., 2006; Wang et al., 2007b, 2012c; Wan et al., 2010; Zhao et al., 2013). The zircon saturation temperature (T_{Zr}) of the granitoids is estimated at 790–839 °C from the measured major element composition and Zr contents (Table S1). Given that the occurrence of inherited zircon cores (Fig. 8a–e) implies a crystallization temperature lower than that required for complete dissolution of zircons (Miller et al., 2003), the estimated T_{Zr} value of 790–839 °C represents an upper limit of recrystallization temperature for the Jiuling granitoids.

5.1.2. The Meixian plutons

Ten samples from the Meixian plutons were analyzed for whole-rock major and trace element compositions (Fig. 2a). Their results are listed in Table S1. Two groups (Groups 1 and 2) can be classified on the basis of their distinct geochemical features. Group 1 samples are granitoids, and show SiO_2 = 65.47–72.4 wt%, Al_2O_3 = 13.93–15.87 wt%, K_2O = 1.99–4.48 wt%, FeOt = 1.46–3.27 wt%, MgO = 0.64–3.39 wt%, CaO = 0.63–3.3 wt%, P_2O_5 = 0.12–0.17 wt%, TiO_2+FeOt+MgO = 2.30–6.87 wt%, K_2O+Na_2O = 5.5–7.67 wt%, and K_2O/Na_2O ratios = 0.57–1.58 (Table S1); they plot in the subalkaline granodiorite and granite fields in the TAS diagram (Fig. 4a). These granitoids have intermediate geochemical features between S-type and I-type granites. They are strongly peraluminous with A/CNK ratios of 1.14–1.36, and fall into the S-type granite field in the triangle diagram of Al_2O_3–(K_2O + Na_2O)–CaO–(FeOt + MgO) (Fig. 4b, c). The high Na_2O contents (2.83–3.88 wt %), together with low K_2O/Na_2O ratios (mostly <1, except for sample Mx159-2), are consistent with geochemical characteristics of I-type granite (Chappell and White, 1974, 1992). In the K_2O–SiO_2 diagram, they plot in the calc-alkaline to high-K calc-alkaline fields (Fig. 5b); they show decreases in Al_2O_3, MgO, FeOt, CaO, and TiO_2 with increasing SiO_2 in Harker diagrams (Fig. 5a, d–f, i). These granitoids have total REE contents of 81–131 ppm, and show steep REE chondrite-normalized patterns with $(La/Yb)_N$ = 7.31–17.34 and $(Gd/Yb)_N$ = 1.60–2.81 (Fig. 6c, Table S1). They are characterized by markedly negative Eu anomalies with Eu/Eu* = 0.69–0.81 (Fig. 6c, Table S1). Such anomalies, together with the plot patterns of Sr versus Ba and Rb (Fig. 7a, b), indicate the fractionation of plagioclase. On the primitive mantle-normalized spidergram (Fig. 6d), they are enriched in Rb, Th and U, and depleted in Ba, Nb, Sr, and Ti, coinciding well with the characters of S-type magmas. The scarce occurrence of inherited zircons (Fig. 8f, g) and extremely low Zr contents (25.78–59.89 ppm, Table S1) indicate that the granitoids did not attain zircon saturation. Therefore, the zircon saturation temperature (T_{Zr}) is not calculated.

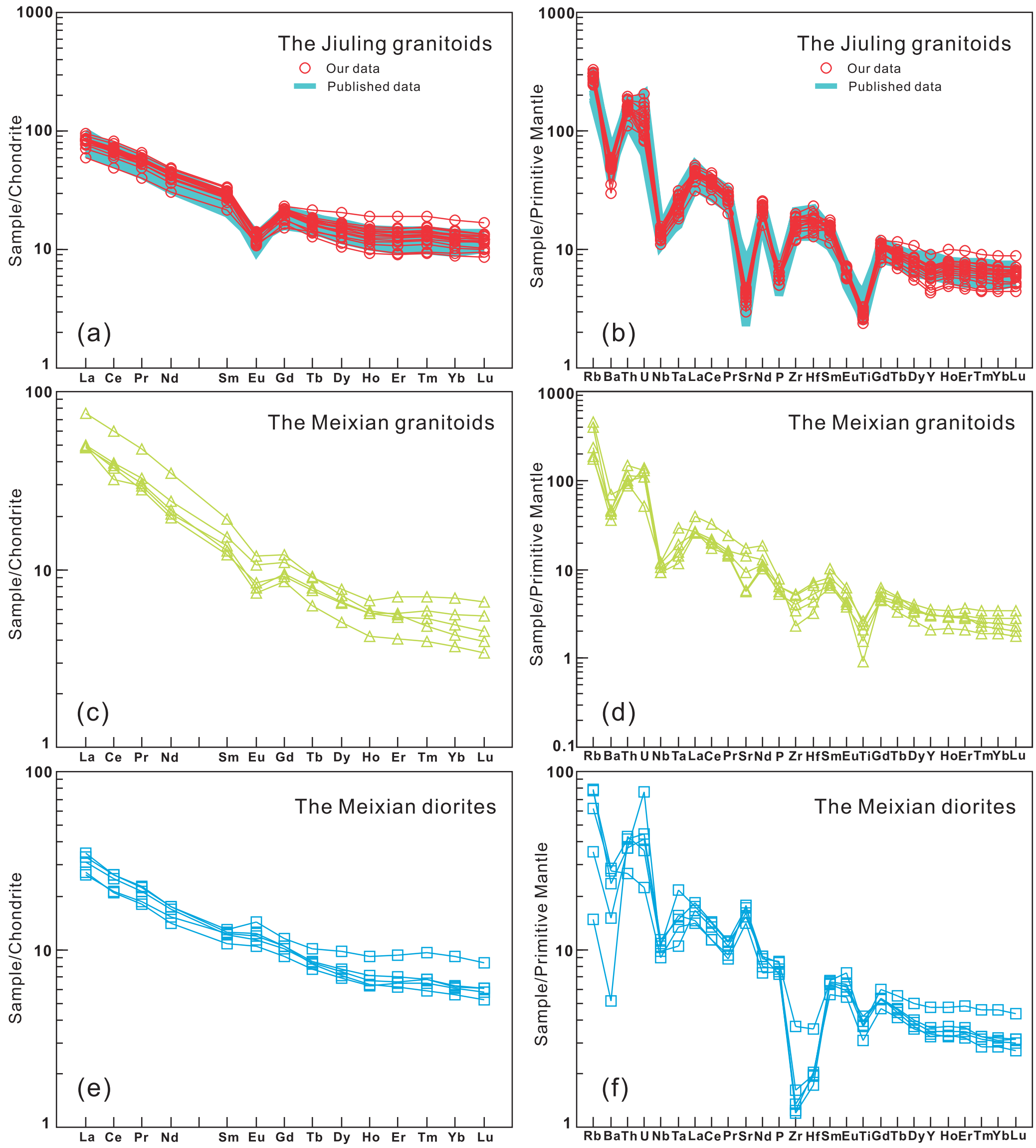

Fig. 6. Chondrite-normalized REE patterns and Primitive mantle-normalized multiple trace element diagrams of the Jiuling and Meixian plutons. Chondrite and primitive mantle normalizing values are from Taylor and McLennan (1985) and Sun and McDonough (1989), respectively. Published data for the Jiuling granitoids (Li et al., 2003a; Wang et al., 2004b) are also indicated.

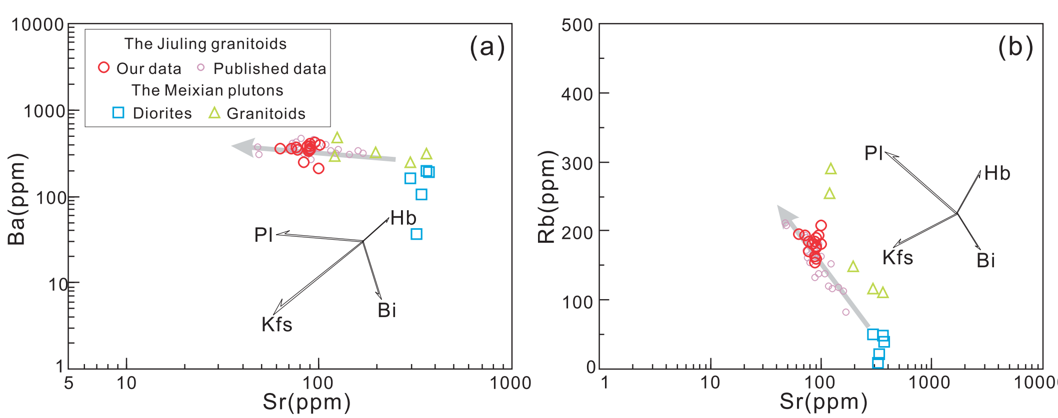

Fig. 7. Sr versus Ba (a) and Sr versus Rb (b) diagrams for the Jiuling and Meixian plutons. Symbols in Fig. 7b are the same as those in Fig. 7a. Published data for the Jiuling granitoids are from Li et al. (2003a) and Wang et al. (2004b). Arrows indicate the influence of fractionation of plagioclase (Pl), K-feldspar (Kfs), hornblende (Hb) and biotite (Bi) on the composition of the residual liquids.

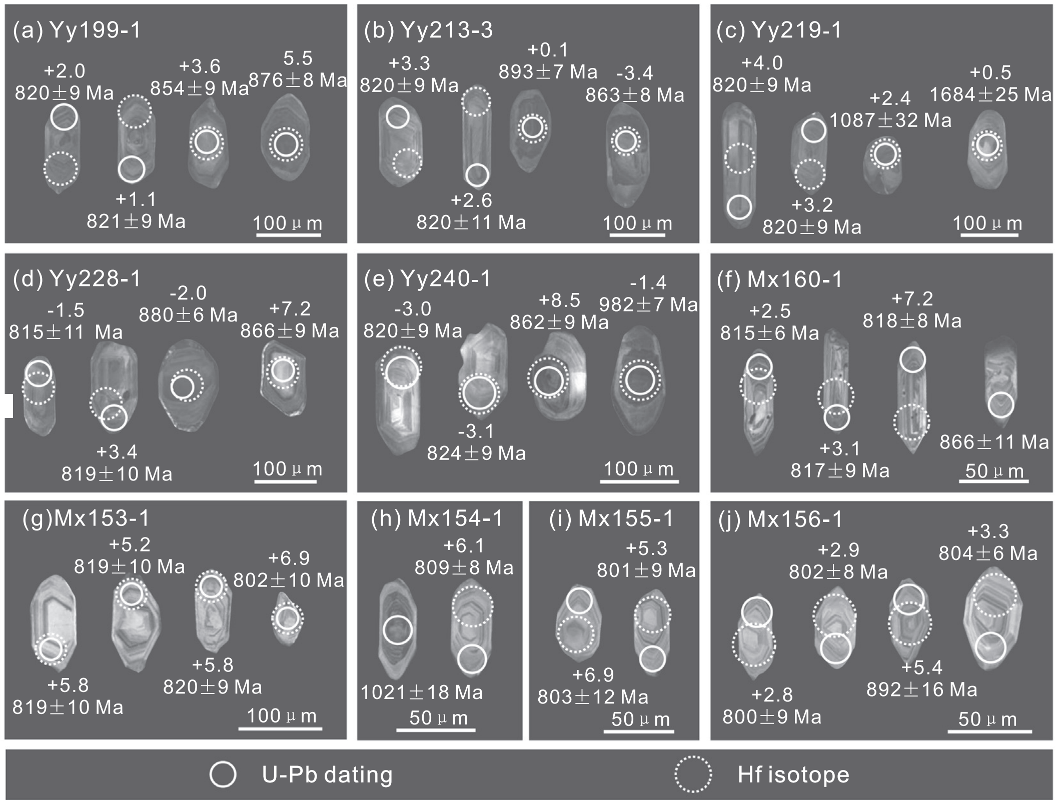

Fig. 8. CL images of representative zircons from the Jiuling and Meixian plutons. Small solid circles are spots for U-Pb isotope analysis, and big white dashed circles are spots for Hf isotope analysis.

Group 2 samples are diorites, and have SiO_2 = 54.28–62.43 wt%, Al_2O_3 = 17.14–19.05 wt%, FeOt = 4.15–5.96 wt%, MgO = 3.00–4.38 wt%, CaO = 4.94–7.6 wt%, P_2O_5 = 0.16–0.19 wt%, TiO_2+FeOt+MgO = 7.81–11.16 wt%, and K_2O+Na_2O = 4.01–4.92 wt% (Table S1); they plot in the subalkaline gabbroic diorite and diorite fields in the TAS diagram (Fig. 4a). These diorites are metaluminous to peraluminous with the A/CNK ratios = 0.93–1.06 (Fig. 4b, Table S1). They have K_2O = 0.25–1.14 wt%, low K_2O/Na_2O ratios (0.07–0.31), and plot in the tholeiitic to calc-alkaline fields in the K_2O–SiO_2 diagram (Fig. 5b). In Harker diagrams, the diorites show decreases in Al_2O_3, MgO, FeOt, and CaO with increasing SiO_2 (Fig. 5a, d–f), whereas P_2O_5 and TiO_2 increase until SiO_2 reaches ~57% and then decrease at higher SiO_2 contents (Fig. 5h–i). These diorites have total REE contents of 56–70 ppm, and show fractionated REE patterns expressed by LREE enrichment and HREE depletion with $(La/Yb)_N$ = 3.62–6.15 (Fig. 6e, Table S1). They show weakly positive Eu anomalies with Eu/Eu* = 1.01–1.17 (Fig. 6e, Table S1). On the primitive mantle- normalized spidergram (Fig. 6f), they are enriched in Rb, Th, U and Sr, and depleted in Ba, Nb, Zr, Hf and Ti, consistent with geochemical characters of arc magmas, which might have reflected inheritance of juvenile arc-derived crust (see below).

5.2. Zircon U-Pb ages

Zircons from ten samples from the Jiuling and Meixian plutons are subhedral, euhedral and long prismatic. They range from 50 to 200 μm in length, and have length/width ratios of ~1.5:1 to 3:1. For the Jiuling plutons, CL imaging shows that (1) most zircon grains exhibit oscillatory zoning, indicative of igneous origin (Fig. 8a–e); and (2) some zircons display a core-rim structure: the highly luminescent cores represent inherited/xenocrystic grains that have been modified by recrystallization; the weakly luminescent rims display oscillatory zoning with euhedral shape, and have resulted from the magmatic overgrowth (Fig. 8a–e). For the Meixian plutons, magmatic oscillatory zonings are common in most zircon grains, with a few grains exhibiting core-rim structure (Fig. 8f–j). All zircon U-Th-Pb isotopic data are shown on concordia diagrams in Fig. 9 and listed in Appendix Table S2.

5.2.1. The Jiuling granitoids

Sample Yy199-1 is a mylonitic granodiorite collected from the southern part of the Jiuling granitoids (Fig. 2a). Thirty-eight analyses were conducted on 38 zircon grains. These zircons have Th contents of 25–640 ppm and U contents of 145–938 ppm, corresponding to Th/U ratios of 0.07–1.46 (Table S2). Among these, twenty-eight analyses are concordant and yield a weighted mean $^{206}Pb/^{238}U$ age of 820 ± 3 Ma (MSWD = 0.03) (Fig. 9a), herein interpreted as the crystallization age of the granodiorite. Spots #29–38 are inherited zircons as identified by their relatively dark CL images (Fig. 8a). Except for three spots (#32, #33 and #35) that yield $^{207}Pb/^{206}Pb$ ages of 1.59–1.87 Ga, the other spots yield $^{206}Pb/^{238}U$ ages of 854–1008 Ma (Fig. 9a, Table S2).

Sample Yy213-3 is a granodiorite collected from the central part of the Jiuling granitoids (Fig. 2a). Zircons from this sample have variable concentrations of U (149–2315 ppm) and Th (23–2337 ppm), with Th/U ratios ranging from 0.08 to 1.05 (Table S2). Thirty concordant analyses yield a weighted mean $^{206}Pb/^{238}U$ age of 820 ± 4 Ma (MSWD = 0.01) (Fig. 9b), which we interpreted as the crystallization age of the granodiorite. In addition, eight inherited/xenocrystic zircon cores surrounded by magmatic rims are identified (Fig. 8b). Among these, six cores (Spots #31–32, #34 and #36–38) yield $^{206}Pb/^{238}U$ ages in the range of 863–927 Ma (Fig. 9b, Table S2), and two cores (Spots #33 and #35) yield older $^{207}Pb/^{206}Pb$ ages of 1750 ± 24 Ma and 1195 ± 37 Ma, respectively (Table S2).

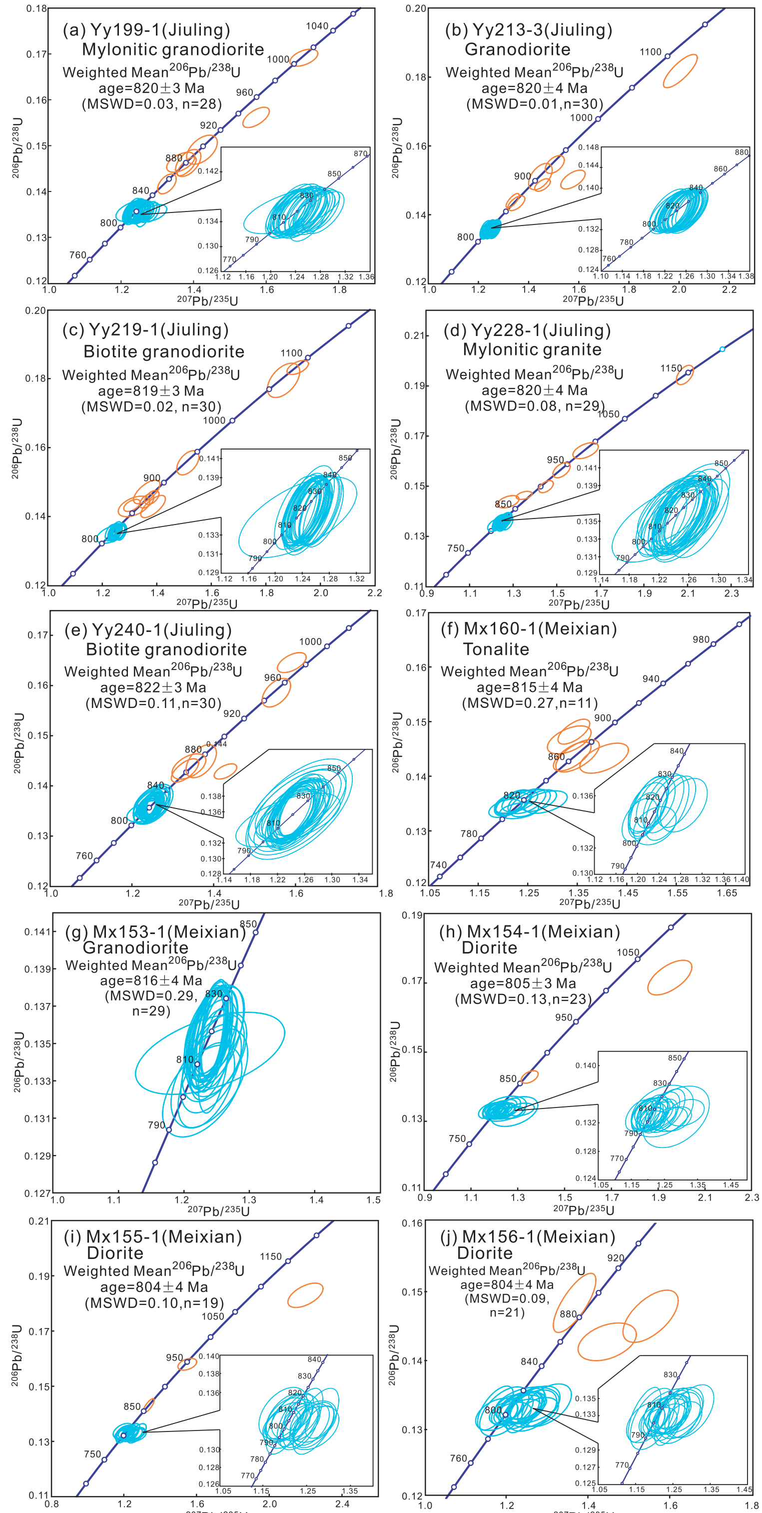

Fig. 9. Concordia diagrams of zircon U-Pb data for samples from the Jiuling and Meixian plutons.

Sample Yy219-1 is a biotite granodiorite collected from the central part of the Jiuling granitoids (Fig. 2a). Zircons from the sample have Th contents from 26 to 449 ppm, U from 82 to 816 ppm, and Th/U ratios from 0.07 to 1.15 (Table S2). Thirty concordant analyses yield a weighted mean $^{206}Pb/^{238}U$ age of 819 ± 3 Ma (MSWD = 0.02) (Fig. 9c), representing the crystallization age of the granodiorite. Spots #31–41 are inherited/xenocrystic cores and zircons (Fig. 8c). Among these, ten spots (Spots #31–40) yield $^{206}Pb/^{238}U$ ages of 861–1085 Ma, and the remaining one spot (Spot #41) yields a $^{207}Pb/^{206}Pb$ age of 1684 ± 25 Ma (Fig. 9c, Table S2).

Sample Yy228-1 is a mylonitic granite collected from the eastern part of the Jiuling granitoids (Fig. 2a). Zircons from this sample have Th contents from 17 to 228 ppm, U contents from 64 to 829 ppm, and Th/U ratios of 0.04–1.42 (Table S2). Among a total of forty analyses, twenty-nine analyses are concordant and define a weighted mean $^{206}Pb/^{238}U$ age of 820 ± 4 Ma (MSWD = 0.08) (Fig. 9d), which is interpreted as the crystallization age of the granodiorite. The remaining eleven spots are inherited/xenocrystic zircon cores, surrounded by narrow rims (Fig. 8d). Five zircon cores (Spots #31–34 and #37) yield $^{206}Pb/^{238}U$ ages of 866–980 Ma, and the other six cores (Spots #11, #35–36, and #38–40) give older $^{207}Pb/^{206}Pb$ ages of 1.15–2.37 Ga (Table S2).

Sample Yy240-1 is a mylonitic granodiorite collected from the eastern part of the Jiuling granitoids (Fig. 2a). Thirty-nine analyses were conducted on 39 zircon grains. Their zircons have Th contents of 28–327 ppm and U contents of 131–954 ppm, with Th/U ratios ranging from 0.15 to 1.01 (Table S2). Thirty concordant analyses define a weighted mean $^{206}Pb/^{238}U$ age of 822 ± 3 Ma (MSWD = 0.11) (Fig. 9e), which we interpreted as the crystallization age of the granodiorite. The other nine analyses (Spots #31–39) are conducted on inherited zircons characterized by relatively dark CL images (Fig. 8e). Except for two spots (#34 and #36) that yield $^{207}Pb/^{206}Pb$ ages of 2350 ± 25 Ma and 1573 ± 26 Ma, respectively, the other spots (#31–33, #35, and #37–39) yield $^{206}Pb/^{238}U$ ages of 860–982 Ma (Table S2).

5.2.2. The Meixian plutons

Sample Mx160-1 is a plagioclase granite collected from the northern part of the Meixian plutons (Fig. 2a). Zircons from this sample have Th and U concentrations of 98–694 ppm and 216–1134 ppm, respectively. Their Th/U ratios range from 0.34 to 1.00 (Table S2). Among a total of sixteen analyses, eleven concordant analyses yield a weighted mean $^{206}Pb/^{238}U$ age of 815 ± 4 Ma (MSWD = 0.27) (Fig. 9f), representing the crystallization age of the plagioclase granite. The remaining five spots (#2, #5, #6, #14, and #15) are inherited zircons (Fig. 8f), and yield $^{206}Pb/^{238}U$ ages of 863–891 Ma (Table S2).

Sample Mx153-1 is a granodiorite collected from the northwestern part of the Meixian plutons (Fig. 2a). Twenty-nine analyses were conducted on 29 zircon grains. These zircons have relatively low concentrations of Th (25–119 ppm) and U (70–231 ppm), with Th/U ratios ranging from 0.24 to 0.62 (Table S2). All the analyses are concordant and define a weighted mean $^{206}Pb/^{238}U$ age of 816 ± 4 Ma (MSWD = 0.29) (Fig. 9g), which is interpreted as the crystallization age of the granodiorite.

Sample Mx154-1 is a diorite collected from the northwestern part of the Meixian plutons (Fig. 2a). Twenty-five analyses were conducted on 25 zircon grains. These zircons have variable Th (53–1524 ppm), U (106–1482 ppm) contents, and Th/U ratios of 0.35–1.03 (Table S2). Twenty-three concordant analyses yield a weighted mean $^{206}Pb/^{238}U$ age of 805 ± 3 Ma (MSWD = 0.13) (Fig. 9h), which we interpreted as the crystallization age of the diorite. Two analyses (#18 and #20) are inherited zircons with high Th (1524 and 438 ppm) and U (1482 and 612 ppm) contents (Fig. 8h, Table S2). They yield a $^{206}Pb/^{238}U$ age of 861 ± 7 Ma and a $^{207}Pb/^{206}Pb$ age of 1220 ± 40 Ma, respectively (Table S2).

Sample Mx155-1 is a diorite collected from the northwestern part of the Meixian plutons (Fig. 2a). Zircons from this sample have Th contents of 48–808 ppm, U contents of 96–923 ppm, and Th/U ratios of 0.12–0.97 (Table S2). Among a total of twenty-two analyses, nineteen analyses are concordant and yield a weighted mean $^{206}Pb/^{238}U$ age of 804 ± 4 Ma (MSWD = 0.10) (Fig. 9i), representing the crystallization age of the diorite. Three analyses (#6, #9 and #14) are inherited zircons, and yield older $^{206}Pb/^{238}U$ ages of 1083 ± 16 Ma, 945 ± 8 Ma and 861 ± 10 Ma, respectively (Table S2).

Sample Mx156-1 is a diorite collected from the northwestern part of the Meixian plutons (Fig. 2a). Its zircons have Th concentrations of 54–374 ppm and U concentrations of 106–456 ppm, corresponding to Th/U ratios of 0.41–0.90 (Table S2). Among a total of twenty-four analyses, twenty-one concordant analyses yield a weighted mean $^{206}Pb/^{238}U$ age of 804 ± 4 Ma (MSWD = 0.09) (Fig. 9j), representing the crystallization age of the diorite. The other three analyses (#10, #12 and #19) are inherited zircons (Fig. 8j), and yield older $^{206}Pb/^{238}U$ ages of 860 ± 10 Ma, 892 ± 16 Ma and 881 ± 14 Ma, respectively (Table S2).

5.3. Zircon Hf isotopes

In situ zircon Hf analyses have been measured on the same grains used for U-Pb dating. Lu-Hf isotope data are shown in Fig. 10a and Fig. 10b–d as plots of the zircon U-Pb ages with respect to their $\varepsilon_{Hf}(t)$ values and histograms of $\varepsilon_{Hf}(t)$ values. Detailed results are listed in Appendix Table S3.

5.3.1. The Jiuling granitoids

Total 116 spots were analysed for zircons from five rock samples from the Jiuling granitoids. Ninety-three analyses were conducted on the magmatic zircons and rims. Among them, eighty-two analyses show positive $\varepsilon_{Hf}(t)$ values, and vary from +0.2 to +8.7 and cluster within the range of +1–+5 (Fig. 10a, b, Table S3). These positive $\varepsilon_{Hf}(t)$ values record a predominant contribution of juvenile crust to the granitoid sources. Their initial $^{176}Hf/^{177}Hf$ ratios range from 0.282266 to 0.282505, corresponding to the depleted mantle two-stage Hf model ages (T_{DM2}) of 1.17–1.71 Ga (Table S3). The other eleven analyses display negative $\varepsilon_{Hf}(t)$ values of −4.2–−0.1 (Table S3), which record a predominant contribution of melting of ancient crustal rocks to the granitoid sources. Their initial $^{176}Hf/^{177}Hf$ ratios are heterogeneous and range from 0.282142 to 0.282257, corresponding to the Hf model ages (T_{DM2}) of 1.73–1.99 Ga (Table S3). Among these spots, the lowest $\varepsilon_{Hf}(t)$ value (−4.2 ± 1.1) occurs in a young zircon with a $^{236}Pb/^{238}U$ age of 820 Ma (Spot #3 in sample Yy228-1), corresponding to the lowest $^{176}Hf/^{177}Hf$ ratio of 0.282142 and the oldest Hf model age (T_{DM2}) of 1990 ± 45 Ma (Table S3).

Twenty-three analyses are conducted on inherited and xenocrystic cores. Among these, fifteen cores with U-Pb ages of 854–982 Ma yield dominantly positive $\varepsilon_{Hf}(t)$ values of 0.1–8.5 (11 spots) and slightly negative $\varepsilon_{Hf}(t)$ values of −3.4–−0.3 (4 spots). Their initial $^{176}Hf/^{177}Hf$ ratios range from 0.282120 to 0.282473, corresponding to the Hf model ages (T_{DM2}) of 1.22–1.98 Ga (Table S3). The remaining eight cores that are dated at 1.0–2.37 Ga show variable $\varepsilon_{Hf}(t)$ values from −9.0 to +12.2 (Table S3). Their initial $^{176}Hf/^{177}Hf$ ratios range from 0.281465 to 0.282318, corresponding to the Hf model ages (T_{DM2}) of 1.47–2.91 Ga (Table S3). The Hf isotope compositions of inherited zircons are comparable with those of detrital zircons within the Shuangqiaoshan Group, in which most 860–980 Ma detrital zircons were derived from the Shuangxiwu volcanic arc (Wang et al., 2013c).

5.3.2. The Meixian plutons

5.3.2.1. The Meixian granitoids. A total of twenty-two spots were analysed for zircon Lu-Hf isotopes of samples Mx153-1 and Mx160-1 from the Meixian granitoids. Except for three negative $\varepsilon_{Hf}(t)$ values of −1.1, −0.2 and −1.6, all 815–816 Ma spots yield positive $\varepsilon_{Hf}(t)$ values from +0.5 to +7.2 (Fig. 10a, c, Table S3), documenting the contribution of juvenile crust to the magma source. Their initial $^{176}Hf/^{177}Hf$ ratios range from 0.282219 to 0.282466, corresponding to the Hf model ages (T_{DM2}) of 1.26–1.82 Ga (Table S3). Among these spots, the lowest $\varepsilon_{Hf}(t)$ value (−1.6 ± 0.4) is associated with the lowest $^{176}Hf/^{177}Hf$ ratio (0.282219), corresponding to the oldest Hf model age (T_{DM2}) of 1820 ± 16 Ma (Spot #16 in sample Mx160-1, Table S3). One inherited zircon dated at 863 ± 10 Ma gives the $\varepsilon_{Hf}(t)$ value of 1.3 ± 0.4 and an initial $^{176}Hf/^{177}Hf$ ratio of 0.282270, corresponding to the Hf model age (T_{DM2}) of 1674 ± 15 Ma (Table S3).

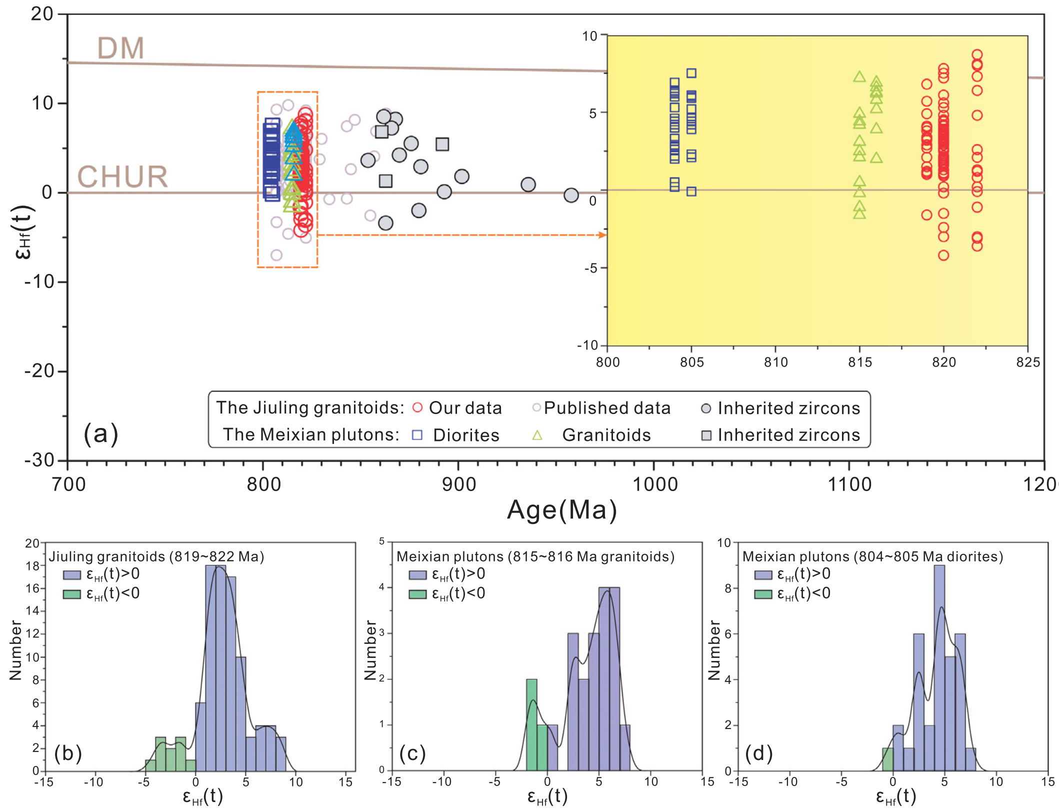

Fig. 10. Hf isotopic compositions of zircons from the Jiuling and Meixian plutons. (a) Zircon $\varepsilon_{Hf}(t)$ values versus zircon U-Pb ages; (b-d) Histograms of zircon $\varepsilon_{Hf}(t)$ values; DM: depleted mantle; CHUR: chondritic uniform reservoir. Published data for the Jiuling granitoids are from Wang et al. (2013b) and Zhao et al. (2013).

5.3.2.2. The Meixian diorites. Total thirty-six analyses were made on zircons from three samples Mx154-1, Mx155-1 and Mx156-1 from the Meixian diorites. Given the nearly same $^{206}Pb/^{238}U$ ages, no significant correlation between the $^{206}Pb/^{238}U$ age and the $^{176}Lu/^{177}Hf$ ratio has been observed (Table S3). Except for one slightly negative $\varepsilon_{Hf}(t)$ value of −0.1, all 804–805 Ma spots show positive $\varepsilon_{Hf}(t)$ values of 0.2–7.5 (Fig. 10a, d, Table S3), reflecting a major mantle contribution from the magma sources. Their initial $^{176}Hf/^{177}Hf$ ratios range from 0.282266 to 0.282483, corresponding to the Hf model ages (T_{DM2}) of 1.23–1.72 Ga (Table S3). Among these spots, the lowest $\varepsilon_{Hf}(t)$ value (−0.1 ± 0.4) is associated with the lowest $^{176}Hf/^{177}Hf$ ratio (0.282266), corresponding to the oldest Hf model age (T_{DM2}) of 1721 ± 17 Ma (Spot #19 in sample Mx154, Table S3). Three inherited zircons, with U-Pb ages of 1328 ± 38 Ma, 861 ± 10 Ma, and 892 ± 16 Ma, yield $\varepsilon_{Hf}(t)$ values of 7.3 ± 0.5, 6.8 ± 0.9 and 5.4 ± 0.4, respectively (Table S3). Their initial $^{176}Hf/^{177}Hf$ ratios range from 0.282145 to 0.282426, corresponding to Hf model ages (T_{DM2}) of 1.32–1.65 Ga (Table S3).

6. Discussion

6.1. Petrogenesis

6.1.1. The Jiuling granitoids

The Jiuling granitoids display intermediate geochemical features between S-type and I-type granites. The S-type affinity is evidenced by high K_2O/Na_2O (1.16–1.50) and A/CNK ratios (1.3–1.45) (Table S1), while the I-type affinity is expressed by extensive occurrence of hornblende (Fig. 3b) and negative correlation between P_2O_5 and SiO_2 (Fig. 5h) (Chappell and White, 1974, 1992). Such features of both S- and I-type affinities indicate isotope disequilibrium, possibly due to source heterogeneity and magma mixing (Valley et al., 1994; Griffin et al., 2002; Valley, 2003; Appleby et al., 2010; Wang et al., 2013b). A mixed origin is consistent with the highly variable zircon $\varepsilon_{Hf}(t)$ values of −4.2–+8.7 (Fig. 10a, b, Table S3) and $\delta^{18}O$ values of 6.9–12‰ (Wang et al., 2013b; Zhao et al., 2013), and can be further traced from the plot of CaO/Na_2O vs Al_2O_3/TiO_2, in which the granitoids fall into the jointed field of the meta-greywacke and meta-igneous sources (Fig. 11a). The above-stated observations indicate that the Jiuling granitoids were generated by melting and binary mixing of juvenile crustal and supracrustal material. Given the crust-mantle mixing, the model Hf age represents an average age of the mixed source, and does not date crustal growth or reworking.

The incorporation of juvenile crustal material in the magma source is indicated by: (1) positive $\varepsilon_{Hf}(t)$ values of 3.8–4.4 for most zircons (Fig. 10b, Table S3); (2) good correlations between TiO_2 and Al_2O_3 with SiO_2 contents (Fig. 5a, i); and (3) high FeOt, MgO and TiO_2 contents and low Al_2O_3/(MgO + FeOt) ratios (Table S1). Notably, most inherited zircons from the granitoids have concordant $^{206}Pb/^{238}U$ ages ranging between 854 ± 9 Ma and 982 ± 7 Ma (Table S2). These ages are consistent with the time (970–880 Ma) of arc-related volcanic rocks in the Shuangxiwu arc (Li et al., 2009), implying that the inherited zircons were likely derived from the Shuangxiwu arc. The Jiuling granitoids exhibit arc-like patterns of REE and trace element partition, expressed by enrichment in LILE (e.g., Rb, Th, U) and LREE, and negative anomalies in P and HFSE (e.g., Nb, Ta, Ti), which were genetically originated from chemical differentiation of arc-derived magmas (Sun and McDonough, 1989; Taylor and Mclennan, 1995). Compared with arc-related volcanic rocks in the Shuangxiwu arc (Li et al., 2009; Yao et al., 2015), the granitoids are more evolved and display more enrichment in LILE (e.g. Rb, Th, U), stronger Nb-Ta negative anomalies

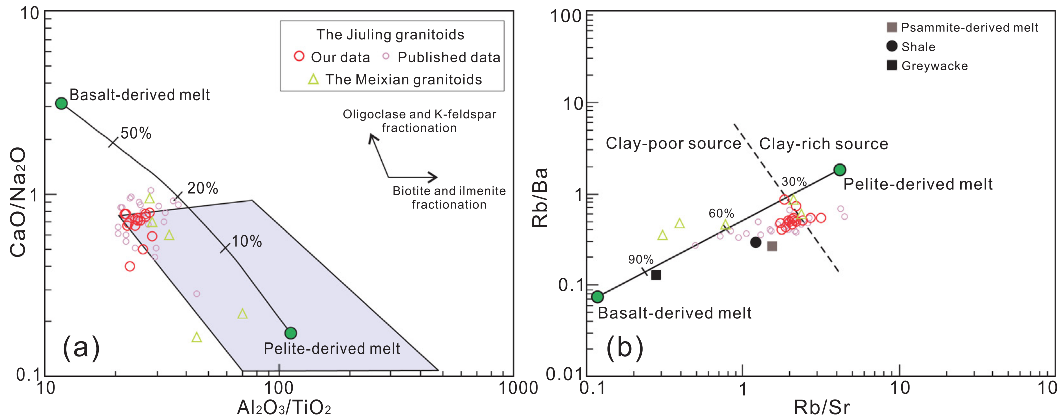

Fig. 11. Plots of (a) Al_2O_3/TiO_2 versus CaO/Na_2O and (b) Rb/Sr versusu Rb/Ba of the Jiuling and Meixian granitoids (after Sylvester, 1998). The mixing curve between the basalt- and pelite-derived melts is from Patino-Douce and Harris (1998) and Sylvester (1998). Published data for the Jiuling granitoids (Li et al., 2003a; Wang et al., 2004b) are also indicated. Symbols in Fig. 11b are the same as those in Fig. 11a.

(Fig. 6a, b), and lower $\varepsilon_{Hf}(t)$ values (−3.4–+8.5) of 854–982 Ma zircons, genetically resulting from potential incorporation of sedimentary components into magma sources during reworking of the juvenile crust (Sun and McDonough, 1989). Accordingly, the arc-like patterns reflect inheritance of juvenile arc-derived crust, with some modification by remelting during crustal reworking.

The Rb/Ba-Rb/Sr plotting illustrates the contributions from melting of a clay-poor, plagioclase-rich, psammitic source (Fig. 11b). The involvement and partial melting of supracrustal material during magma generation have also been supported by four following lines of evidence: (1) low Rb/Sr (1.75–3.13) and high CaO/Na_2O (>0.6) ratios (Table S1); (2) xenoliths of sedimentary rocks within the granitoids (Zhao et al., 2013); (3) neutral to negative $\varepsilon_{Nd}(t)$ values (−0.2–−3.1) of the granitoids (Li et al., 2003a); and (4) high $\delta^{18}O$ values (7.0–10.6‰) of zircons from the granitoids (Wang et al., 2013b; Zhao et al., 2013). Our geochronological data define four groups of inherited/xenocrystic zircons: a major group at ~860–970 Ma, and three minor groups at ~1.1–1.2 Ga, ~1.5–1.8 Ga and ~1.9–2.37 Ga, respectively (Table S2). Such an age pattern is temporally consistent with detrital zircon records of the granitoid country supracrustal rocks, i.e., the meta-sedimentary rocks of the Shuangqiaoshan Group (Wang et al., 2013c). The Shuangqiaoshan meta-sedimentary rocks contain numerous 850–970 Ma detrital zircons, which display high positive $\varepsilon_{Hf}(t)$ values close to that of the contemporary depleted mantle (Wang et al., 2013c). Such zircons were illustrated to be derived from the Shuangxiwu arc magmas (Wang et al., 2013c), implying that the Shuangxiwu arc underwent significant erosion and shed detritus to the basin where the Shuangqiaoshan Group was deposited (Wang et al., 2008a; Wang and Zhou, 2013). The occurrence of ~1.1–1.2 Ga, ~1.5–1.8 Ga and ~1.9–2.37 Ga zircons within the Jiuling granitoids reflects inheritance from detrital zircons within the Shuangqiaoshan meta-sedimentary rocks (Wang et al., 2013c). The ~1.1–1.2 Ga zircons were possibly derived from the ~1160 Ma alkaline bimodal volcanic rocks of the Tieshajie Group (Li et al., 2013), and the ~1.5–1.8 Ga and ~1.9–2.37 Ga zircons were sourced from the recycled Mesoproterozoic to Paleoproterozoic material within the Tianli schist (Li et al., 2007; Wang et al., 2013c). In addition, the $\varepsilon_{Nd}(t)$ values for the Jiuling granitoids (−0.2~−3.1, Li et al., 2003a) are compatible with those (−0.4–−2.5) of the Shuangqiaoshan Group (Chen and Jahn, 1998). The age consistency and isotopic similarity indicate that the generation of the Jiuling granitoids was closely associated with partial melting of the meta-sedimentary rocks of the Shuangqiaoshan Group. The time interval between the Jiuling granitoid emplacement (~825–815 Ma) and the Shuangqiaoshan Group deposition (<850 Ma, Wang et al., 2013c) is less than 20 Ma, similar to that in the Lachlan Fold Belt of southeastern Australia, where the 430–410 Ma S-type granites were melted from <443 Ma sediments that the granites intrude (Keay et al., 1999).

On the basis of the above discussion, we interpret that the Jiuling granitoids were produced by remelting and binary mixing of (1) juvenile arc-derived crustal material and (2) supracrustal material of the Shuangqiaoshan meta-sedimentary rocks. Coeval remelting of the juvenile arc-derived crust has also been documented in the eastern Jiangnan Orogen (Wu et al., 2006; Zheng et al., 2008; Wang et al., 2012a). Therefore, we infer that Neoproterozoic remelting of juvenile crust is a regional-scale event across the Jiangnan orogen, which might have led to substantial increase of continental component in the bulk crust composition (Wu et al., 2006).

6.1.2. The Meixian granitoids

The Meixian granitoids share common features in element and isotope geochemistry with the Jiuling granitoids, particularly in geochemical characteristics of both S-type (Fig. 4b, c) and I-type granites (e.g., high Na_2O contents and low K_2O/Na_2O ratios of 0.57–0.98, Table S1), as well as arc-like patterns of REE and trace element partition (Fig. 6c, d) and highly variable Hf isotope ratios (Fig. 10a, c). The geochemical features of the Meixian granitoids herald mixed meta-sedimentary and meta-igneous sources buried in the deep crust before anatexis. The arc-like patterns are interpreted to be inherited from pre-existing arc-derived rocks. The highly variable $\varepsilon_{Hf}(t)$ values of −1.6–+7.2 testify to isotope disequilibrium associated with magma mixing (Fig 10a, c, Table S3). A mixed trend can also be traced from the Rb/Ba-Rb/Sr and CaO/Na_2O-Al_2O_3/TiO_2 plots (Fig. 11a, b), in which the involvement of two end-members in magma sources is revealed. Given the above-stated isotopic similarity with the Jiuling granitoids, we argue for a consistent binary mixing origin for the Meixian granitoids, i.e., the remelting of supracrustal (i.e., the Shuangqiaoshan meta-sedimentary rocks) and juvenile arc-derived crustal material.

6.1.3. The Meixian diorites

All zircons expect one from the Meixian diorites have positive $\varepsilon_{Hf}(t)$ values of +0.2–+7.5 (Fig. 10d, Table S3), indicating that the diorites might have been generated by differentiation of mantle-derived mafic magmas or mafic crustal material (e.g., Zhao et al., 2010, 2013). In general, the diorite related to mantle-derived magmatism is characterized by high MgO, Cr and Ni contents (MgO > 6 wt%, Cr and Ni each >100 ppm; Smithies and Champion, 2000). By comparison, the Meixian diorites have much lower

MgO (3–4.38 wt%), Cr (60–92.84 ppm) and Ni (57.2–90.37 ppm) contents (Table S1), indicating that they were likely derived from mafic crustal material, rather than mantle-derived magmas. The mafic crust-derived interpretation for the magma sources is also favored by the close similarity between zircon $\varepsilon_{Hf}(t)$ values of the diorites (0.2–7.5) and the arc-related mafic rocks (1.1–7.5 for the Daolinshan dolerite, Yao et al., 2014a; 4.9–12.3 for the Yuanbaoshan mafic rocks, Yao et al., 2014b; 3.4–9.8 for the Miaohou gabbro, Xia et al., 2015).

Previous study has revealed a proportionally greater contribution of the 970–860 Ma arc magmatism to Neoproterozoic juvenile crustal growth (Li et al., 2009). The Meixian diorites display geochemical features similar to arc-related basalts in the Shuangxiwu arc (Li et al., 2009), as expressed by high Al_2O_3 and Na_2O, low MgO and TiO_2, enrichment in LREE and Th, and depletion in Nb, Zr-Hf, and Ti (Fig. 6e, f and Table S1). Six inherited zircons from the diorites yield $^{206}Pb/^{238}U$ ages of 860–945 Ma (Table S2) consistent with the time of the Shuangxiwu arc (Li et al., 2009), indicating that these zircons were derived from arc-related volcanic rocks. The age similarity and arc-like trace element patterns indicate that the Meixian diorites were likely produced by partial melting of juvenile arc-derived mafic crust. Compared with the 815–816 Ma Meixian granitoids, the Meixian diorites are slightly younger and represent products of partial melting of juvenile arc-derived crust at a later stage. The heat that induced partial melting might have been supplied by asthenospheric mantle upwelling during crustal extension.

6.2. Tectonic implications

Increasing evidence shows that the Neoproterozoic development of South China involved oceanic subduction, trench-arc-back-arc system generation, arc-continent collision and post-collisional extension (Wang et al., 2007a, 2008a, 2013a, 2013c, 2014a; Zhou et al., 2009; Shu et al., 2011; Zhang et al., 2012b, 2013; Li et al., 2016b; Zhang and Wang, 2016). Previous studies demonstrated that the Neoproterozoic tectonic evolution of South China was manifested by the generation of three arc-related systems, i.e., the Panxi-Hannan arc-related system (e.g., Zhou et al., 2002a,b; Zhou et al., 2006a,b), the Shuangxiwu arc and back-arc basin system (Ye et al., 2007; Li et al., 2009; Wang et al., 2013c; Yao et al., 2015, 2016b), and the Wuyi-Yunkai arc and back-arc basin system (Zhang et al., 2012c; Wang et al., 2013a, 2014a). We made a summary by synthesizing all published petrological, geochronological and geochemical data of Neoproterozoic magamtic rocks in South China, which are shown in Fig. 14 and listed in Appendix Table S5. In the Jiangnan and Cathaysia domains, the early Neoproterozoic (980–860 Ma) tectonic development of the Shuangxiwu and Wuyi-Yunkai arc-back-arc assemblages requires the divergent double-sided subduction of their intervening oceanic lithosphere, similar to the subduction processes that led to ocean closure in the central Asian orogenic belt (e.g., Xiao et al., 2003, 2015). Detailed discussion on the 980–860 Ma tectonic evolution is beyond the scope of this paper. The following discussion mainly focuses on the mid-Neoproterozoic (830–740 Ma) tectonic evolution of South China.

6.2.1. The ca. 830–825 Ma oceanic basin closure associated with the Yangtze-Cathaysia collision

The development of the Shuangxiwu oceanic basin was manifested by two ophiolitic suites exposed in the Zhangshudun-Xiwan and Fuchuan areas, respectively (Chen et al., 1991; Li et al., 1994, 2008; Li and Li, 2003; Ding et al., 2008; Gao et al., 2009; Zhang et al., 2012b; Yin et al., 2013; Wang et al., 2015). Gabbros from the Zhangshudun-Xiwan ophiolite yield a Sm-Nd mineral internal isochron age of 1034 ± 24 Ma (Chen et al., 1991) that dates the oceanic basin development (Li et al., 2008). Adakitic granites from the Zhangshudun-Xiwan ophiolite were formed by partial melting of the subducted oceanic crust; their SHRIMP U-Pb zircon ages of ca. 970 Ma are interpreted as the timing of subduction of the oceanic crust in the basin (Li et al., 1994; Li and Li, 2003; Gao et al., 2009). High-pressure metamorphic blueschists, formed at ca. 866 ± 14 Ma in the Zhangshudun-Xiwan ophiolite zone (Shu et al., 1993), are considered as recording the subduction of the oceanic crust (Zhao, 2015). The Fuchuan ophiolites, dated at 860–833 Ma Ma (Ding et al., 2008; Yin et al., 2013; Cui et al., 2017), were formed by partial melting of the enriched mantle wedge in the oceanic back-arc basin (Zhang et al., 2012b). In addition, the ca. 860–838 Ma mafic lavas record melting of MORB-like sources and slab-derived fluids in a back-arc basin setting (Zhang et al., 2013). The Shuangxiwu oceanic basin accommodated sedimentation of thick turbidites, in which the Shuangqiaoshan Group that consists of detritus derived from the Shuangxiwu arc, Tianli and Tieshajie highlands was deposited (Wang et al., 2008a, 2013c; Wang and Zhou, 2013; Xu et al., 2014).

During the late filling stage, the Shuangxiwu oceanic basin underwent a dramatic facies transition, with deep-water turbidites

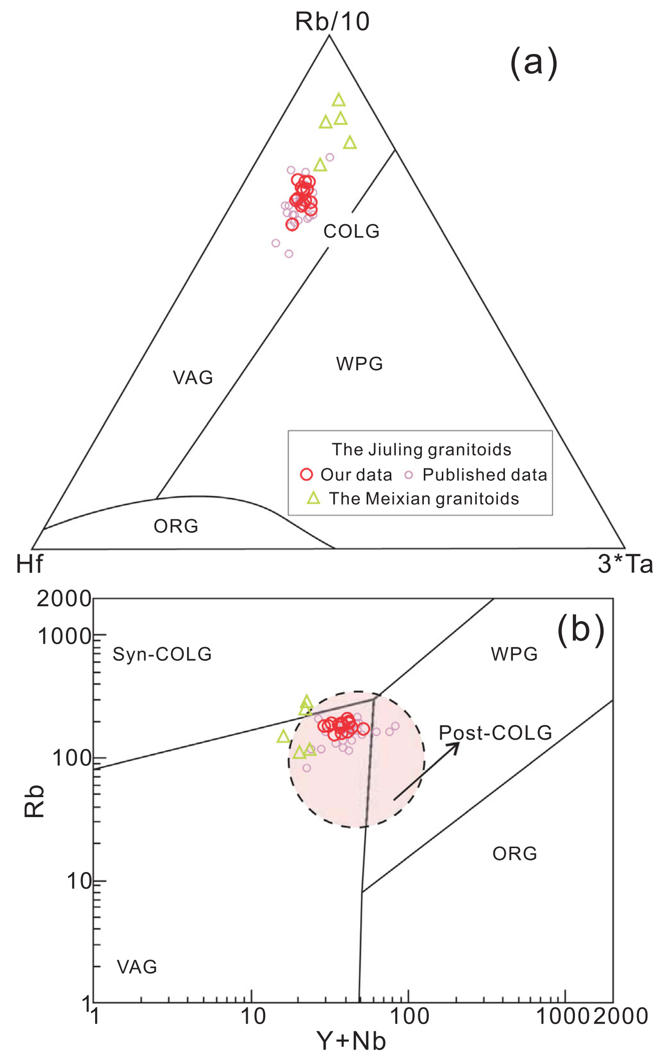

Fig. 12. Tectonic setting discrimination diagrams: (a) Rb/10-Hf-3*Ta diagram is after Harris et al. (1986); (b) (Y + Nb)-Rb diagram is after Pearce (1996) and Pearce et al. (1984). VAG, volcanic arc granite; ORG, ocean ridge granite; WPG, within plate granite; syn-COLG and post-COLG, syn- and post-collision granite; COLG, collision granite. Published data for the Jiuling granitoids (Li et al., 2003a; Wang et al., 2004b) are also indicated. Symbols in Fig. 12b are the same as those in Fig. 12a.

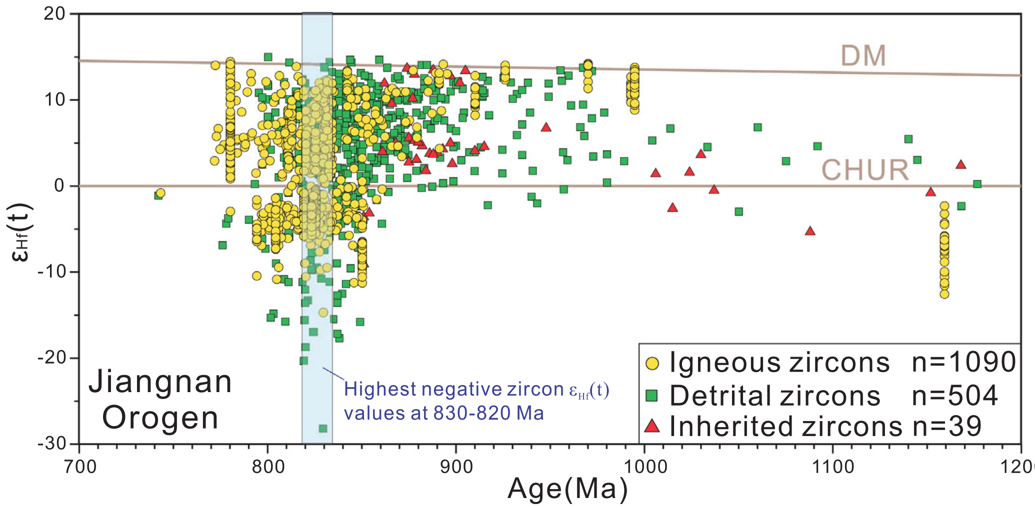

Fig. 13. Compilation of all published zircon $\varepsilon_{Hf}(t)$ versus U-Pb ages in the Jiangnan Orogen. See Table S4 for data sources. DM-depleted mantle; CHUR-chondritic uniform reservoir. Note the highest negative $\varepsilon_{Hf}(t)$ values at 830–820 Ma, which imply the greatest crustal input into the magma sources, corresponding to extreme crustal thickening before extensional collapse and hence heralding the tectonic switch scenario.

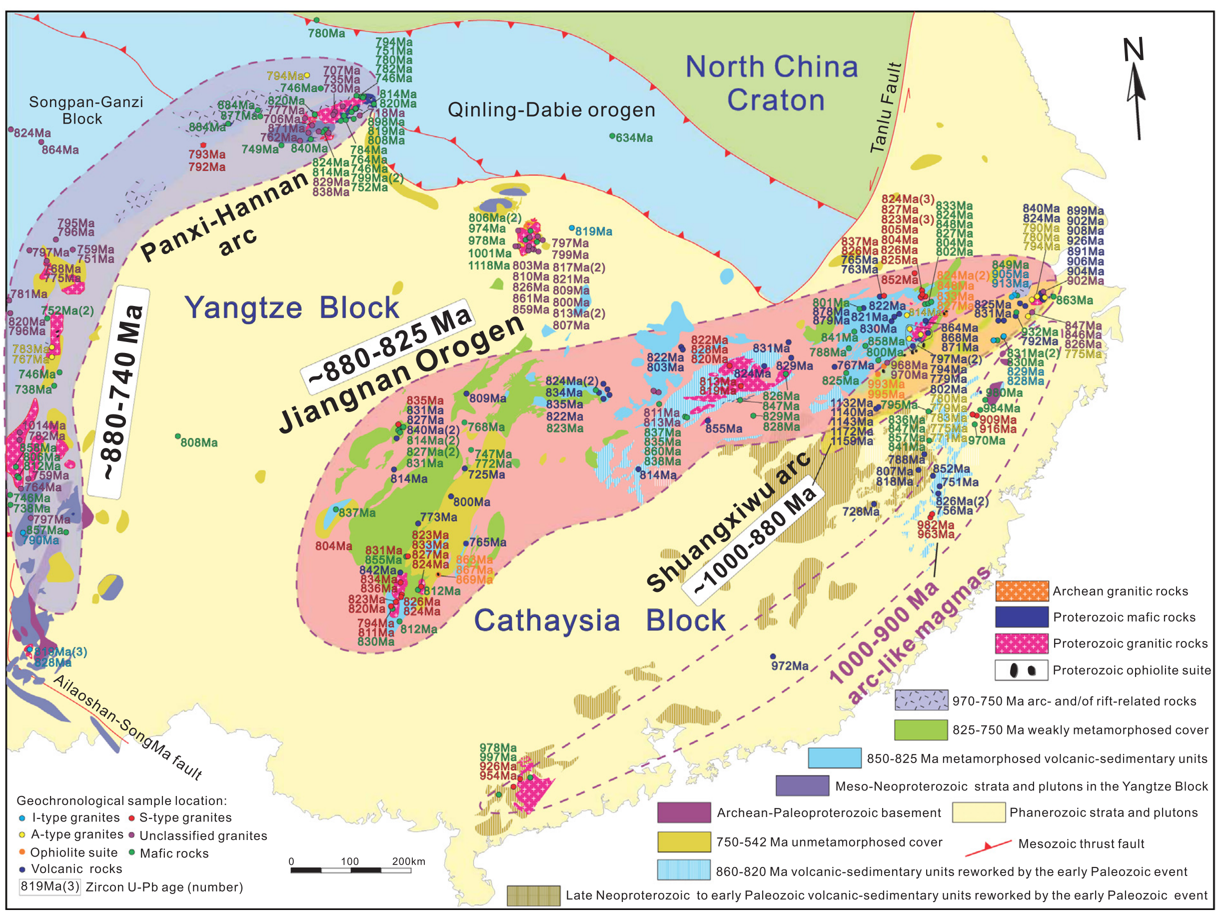

Fig.14. Sketch map showing the ages and distributions of Proterozoic igneous rocks in South China. The division of arc-related systems follows Wang et al. (2014a). The corresponding ages, methods, locations and references are listed in Table S5.

passing upward to fluvial conglomerates (Wang et al., 2013c). The shallowing-up transition represents a flysch-molasse facies change. Such a change records tectonic transition from an extensional basin to a retro-arc foreland basin setting (Wang et al., 2013c), corresponding to tectonic inversion of the basin. Sediment infilling in the retro-arc foreland basin was accommodated by flexural subsidence due to topographic loads of thrust structures. Structural observations manifesting tectonic inversion of the extensional basin are the ubiquitous tight folds and thrusts that involve the Shuangqiaoshan Group and its equivalents (Wang et al., 2007a, 2016; Dong et al., 2015). The folds and thrusts are unconformably overlain by flat-lying flysch turbidites of the Banxi Group and its equivalents (Wang and Li, 2003; Wang et al., 2007a; Gao et al., 2008, 2011). The unconformity is visible on a regional scale, and corresponds to a crustal shortening event that led to final closure of the oceanic basin. Below the unconformity, the youngest bentonite interbedded within the Lengjiaxi Group has been dated at ca. 829 Ma using SHRIMP and SIMS U-Pb zircon methods (Gao et al., 2011; Zhang et al., 2012a, 2015b). Directly above the unconformity, the tuff, bentonite and volcanic interlayers yield U-Pb zircon ages of ca. 814–760 Ma (Wang, 2003; Zhang et al., 2008a,b; Gao et al., 2010, 2011, 2015). These geochronological data place the time of crustal thickening associated with the oceanic basin closure between ca. 829 and 814 Ma (Fig. 15a). The closure of the oceanic basin led to final collision of the Yangtze and Cathaysia blocks (Fig. 15a). Such a collision possibly marks a terminal episode of amalgamating Rodinia in South China (Zheng et al., 2008).

6.2.2. The ca. 825–815 Ma S-type granitoid emplacement that heralded post-collisional extensional collapse of thickened crust

The closure of the oceanic basin was followed by ca. 825–815 Ma emplacement of the Jiuling and Meixian S-type granitoids. The Jiuling and Meixian granitoids plot exclusively within the collision-related domain on the Rb/10-Hf-Ta×3 diagram (Fig. 12a) and the post-collisional field on the Y+Nb versus Rb diagram (Fig. 12b), supporting interpretation of granitoid emplacement in a post-collisional tectonic setting. Similar post-collisional S-type granitoids are widespread throughout the Jiangnan Orogen (e.g., Li et al., 2003a; Wu et al., 2006; Zheng et al., 2007; Yao et al., 2014b). Zircon U-Pb dating on these granitoids yields ages of ca. 825–815 Ma, including: ca. 823 Ma for the Xucun granodiorite (Li et al., 2003a; Xue et al., 2010), ca. 824–823 Ma for the Shexian granodiorite (Wu et al., 2006), ca. 825–824 Ma for the Xiuning granodiorite (Xue et al., 2010), ca. 830–815 Ma for the Zhaigun, Bendong, Dongma, Sanfang, and Yuanbaoshan granitoids in northern Guangxi (Wang et al., 2006a; Zheng et al., 2007; Zhao et al., 2011, 2013; Yao et al., 2014b). We emphasize that crustal thickening of the preexisting, sediment-dominated basin is a prerequisite for the S-type granitoid generation, which might have been achieved by the Yangtze-Cathaysia collision. Post-collisional extensional collapse of the thickened crust would lead to delamination of crustal roots and underplating of the asthenospheric basalts (Vauchez et al., 1997; Dewey, 1988; Tommasi and Vauchez, 2001; Zheng et al., 2007). Rising of hot asthenospheric material might have supplied heat that caused melting of the thickened, meta-sedimentary and juvenile arc-derived crust, producing the abundant S-type granitoids.

The Jiuling and Meixian granitoids, together with regional 825–815 Ma S-type granitoids, herald post-collisional collapse of thickened crust and mark the onset of crustal extension in the Jiangnan Orogen. In this regard, a significant tectonic switch from compression to extension occurring at ca. 825 Ma could be traced. Regional tight folds and thrusts below the Banxi/Lengjiaxi unconformity, together with molasse deposits in the upper Shuangqiaoshan Group (Wang et al., 2013c), testify to the >825 Ma syn-collisional crustal thickening (Wang et al., 2007a, 2008a). The <820 Ma sedimentary sequences, mafic rocks and bimodal volcanic rocks show evidence of post-collisional crustal rifting (e.g., Wang and Li, 2003; Wang et al., 2012a), reinforcing the tectonic switch.

In addition, the tectonic switch is registered by the marked shift of the zircon Hf arrays at ca. 820 Ma in the $\varepsilon_{Hf}(t)$-time histogram (Fig. 13), whereby zircons with ages of ~830–820 Ma display a large spread and variable $\varepsilon_{Hf}(t)$ values from −28 to +12 (Appendix Table S4), and can be clearly distinguished from the other zircons by the highest negative $\varepsilon_{Hf}(t)$ values. The large $\varepsilon_{Hf}(t)$ variation probably stems from a varying degree of hybridization and/or assimilation between mantle-derived juvenile magmas and crust-derived material during zircon crystallization (Han et al., 2016). The highest negative $\varepsilon_{Hf}(t)$ values imply the greatest crustal input into the magma sources, corresponding to extreme crustal thickening before extensional collapse and hence heralding the tectonic switch scenario.

6.2.3. The ca. 815–740 Ma continental rifting associated with lithospheric extension

Following tectonic emplacement of the ca. 825–815 Ma S-type granitoids, the 805–804 Ma Meixian diorites represent an outcome of post-collisional extension development at a later stage. Such post-collisional extension might have lasted till at least 740 Ma, during which large-scale taphrogenic and magmatic activities occurred, generating the huge Nanhua basin (Wang and Li, 2003). Within the basin, the depositional sequences of fluvial to lacustrine documented four episodes of rifting at 815 Ma, 800 Ma, 780–750 Ma, and <750 Ma, respectively (Wang and Li, 2003). Coeval with crustal subsidence was voluminous magmatism that produced a large number of A-/I- and OIB-type igneous rocks. Examples include: the 794–771 Ma A-type granites and granodiorites in the Daolingshan and Shiershan of the eastern Jiangnan Orogen (Li et al., 2003b; Zheng et al., 2008; Wang et al., 2010b; Xue et al., 2010; Yao et al., 2014a); the 819–748 Ma A- and I-type granites, granodiorites, monzogranites, and bimodal plutons in the Kangdian rift of west Yangtze (Zheng et al., 2007; Huang et al., 2008); and the 814–725 Ma bentonite, rhyolite, tuff, and bimodal

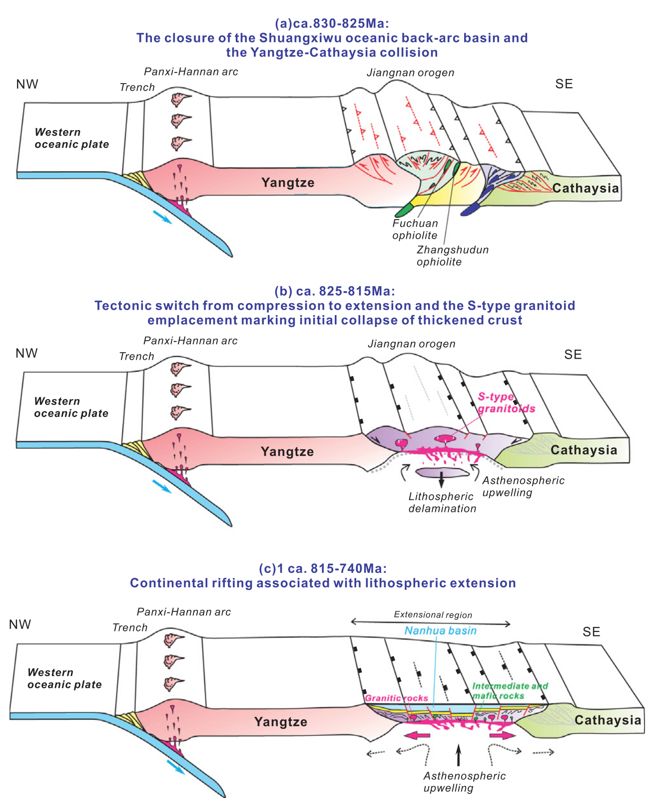

Fig. 15. A tectonic model for Neoproterozoic (830–740 Ma) development of South China, involving the oceanic basin closure, the Yangtze-Cathaysia collision, post-collisional collapse of the thickened crust and lithospheric extension. (a) The 830–825 Ma closure of the oceanic basin and the Yangtze-Cathaysia collision/amalgamation; (b) The 825-815 Ma tectonic switch from compression to extension and S-type granitoid emplacement marking initial collapse of thickened crust; (c) The 815–740 Ma continental rifting associated with lithospheric extension. See Section 6.2 for detailed discussion on (a)–(c).

volcanic rocks in the Jiangnan and Cathaysia domains (Li et al., 2003b, 2008c; Zhang et al., 2008a,b; Gao et al., 2010, 2014b, 2015; Wang et al., 2012a).

The extensive occurrence of the above-stated magmatic rocks testifies to remarkable mid-Neoproterozoic (ca. 815–740 Ma) continental rifting. The rifting had a profound influence on the evolution of South China, and led to continental lithospheric thinning, as expressed by the melting of lithospheric mantle and significant addition of mantle-derived materials into continental crust (Zheng et al., 2007, 2008). The lithospheric thinning or removal might create the accommodation space required for the rise of asthenospheric material. The resultant decompression melting of asthenospheric mantle and partial melting of lithospheric mantle produced the mantle-derived magmas (McKenzie and Bickle, 1988). Underplating of these hot mantle-derived magmas would result in partial melting of the low crust to form extensive intermediate and felsic magmas (Fig. 15c). Such rifting-related processes explained the lithologically variable but genetically linked 815–740 Ma magmatic rocks across the Jiangnan Orogen (Fig. 15c). Given the time consistency, this rifting event may be part of global Neoproterozoic rifting events that finally led to breakup of the Rodinia supercontinent (Zheng et al., 2007, 2008).

7. Conclusions

New data from this study enable us to draw the following conclusions:

(1) The Jiuling and Meixian granitoids display intermediate geochemical features between S-type and I-type granites, and arc-like patterns of REE and trace element partition. Igneous zircons from the granitoids are dated at 822–815 Ma. Most inherited zircons cluster around 980–860 Ma, consistent with the time of the Shuangxiwu volcanic arc. The igneous and inherited zircons exhibit highly variable $\varepsilon_{Hf}(t)$ values of −9–+12.2. These observations support that the granitoids were formed by remelting and binary mixing of (1) juvenile arc-derived crustal material and (2) supracrustal material of the Shuangqiaoshan meta-sedimentary rocks.

(2) The Meixian diorites are dated at 805–804 Ma. They display arc-like geochemical characteristics and have 860–945 Ma inherited zircons with $\varepsilon_{Hf}(t)$ values of −0.1–+7.5, probably reflecting inheritance from the Shuangxiwu volcanic arc. We interpret the Meixian diorites to have been formed by partial melting of the arc-derived lower crust.

(3) The 822–815 Ma granitoids herald post-collisional collapse of thickened crust and mark the onset of crustal extension. The 804–805 Ma diorites, as an outcome of crustal extension development at a later stage, formed in response to continental rifting associated with lithospheric extension.

Acknowledgements

Data supporting this article are either included as supporting information or are available by contacting the corresponding author. This work was financially supported by a Natural Science Foundation of China (NSFC) Project (41190075) entitled "Final Closure of the Paleo-Asian Ocean and Reconstruction of East Asian Blocks in Pangea," which is the fifth research project of NSFC Major Program (41190070) "Reconstruction of East Asian Blocks in Pangea", Hong Kong RGC GRF (HKU7063/13P and 17301915), and a NSFC Project (No. 41502197), Basic Science Foundation of Institute of Geomechanics (No. DZLXJK201601), and Chinese Geological Survey Project (No. 12120115069501). We appreciate the Editor and two anonymous reviewers for their critical, careful, and very constructive reviews that have helped improve the clarity and interpretations of the original draft. Thanks are given to Dr. Yigui Han and Dr. Pengfei Li for their useful comments. Jianhua's work in Hong Kong has been supported by grants from Hong Kong Scholars Program.

Appendix A. Supplementary data

Supplementary data associated with this article can be found, in the online version, at http://dx.doi.org/10.1016/j.precamres.2017.03.018.

References

Andersen, T., 2002. Correction of common lead in U-Pb analyses that do not report ^{204}Pb. Chem. Geol. 192, 59–79.

Appleby, S.K., Gillespie, M.R., Graham, C.M., Hinton, R.W., Oliver, G.J.H., Kelly, N.M., 2010. Do S-type granites commonly sample infracrustal sources? New results from an integrated O, U-Pb and Hf isotope study of zircon. Contrib. Miner. Petrol. 160, 115–132.

Blichert-Toft, J., Albarède, F., 1997. The Lu-Hf isotope geochemistry of chondrites and the evolution of the mantle-crust system. Earth Planet. Sci. Lett. 148, 243–258.

Chappell, B.W., White, A.J.R., 1974. Two contrasting granite types. Pac. Geol. 8, 173–174.

Chappell, B.W., White, A.J.R., 1992. I- and S-type granites in the Lachlan Fold Belt. Trans. R. Soc. Edinb. Earth Sci. 83, 1–26.

Charvet, J., Shu, L.S., Shi, Y.S., Guo, L.Z., Fature, M., 1996. The building of south China: collision of Yangzi and Cathaysia blocks, problems and tentative answers. J. SE Asian Earth Sci. 13, 223–235.

Chen, J.F., Foland, K.A., Xing, F.M., Xu, X., Zhou, T.X., 1991. Magmatism along the southeast margin of the Yangtze block: Precambrian collision of the Yangtze and Cathysia blocks of China. Geology 19, 815–818.

Chen, J.F., Jahn, B.M., 1998. Crustal evolution of southeastern China: Nd and Sr isotopic evidence. Tectonophysics 284, 101–133.

Chu, Y., Lin, W., 2014. Phanerozoic polyorogenic deformation in southern Jiuling massif, northern South China block: constraints from structural analysis and geochronology. J. Asian Earth Sci. 86, 117–130.

Clemens, J., 2003. S-type granitic magmas—petrogenetic issues, models and evidence. Earth Sci. Rev. 61, 1–18.

Cui, X., Zhu, W.B., Fitzsimons, I.C.W., Wang, X., Lu, Y.Z., Wu, X.H., 2017. A possible transition from island arc to continental arcmagmatism in the eastern Jiangnan Orogen, South China: insights from a Neoproterozoic (870–860 Ma) gabbroic-dioritic complex near the Fuchuan ophiolite. Gondwana Res. 46, 1–16.

Dewey, J.F., 1988. Extensional collapse of orogens. Tectonics 7, 1123–1139.

Ding, B.H., Shi, R.D., Zhi, X.C., Zheng, L., Chen, L., 2008. Neoproterozoic (~850 Ma) subduction in the Jiangnan Orogen :evidence from the SHRIMP U-Pb dating of the SSZ-type ophiolite in southern Anhui Province. Acta Petrol. ET Mineral. 27, 375–388 (in Chinese with English Abstract).

Dong, S.W., Zhang, Y.Q., Gao, R., Su, J.B., Liu, M., Li, J.H., 2015. A possible buried Paleoproterozoic collisional orogen beneath central South China: evidence from seismic-reflection profiling. Precambr. Res. 264, 1–10.

Gao, J., Klemd, R., Long, L., Xiong, X., Qian, Q., 2009. Adakitic signature formed by fractional crystallization: an interpretation for the Neo-Proterozoic meta-plagiogranites of the NE Jiangxi ophiolitic mélange belt, South China. Lithos 110, 277–293.

Gao, L.Z., Yang, M.G., Ding, X.Z., Liu, Y.X., Liu, X., Ling, L.H., Zhang, C.H., 2008. SHRIMP U-Pb zircon dating of tuff in the Shuangqiaoshan and Heshangzhen groups in South China: constraints on the evolution of the Jiangnan Neoproterozoic orogenic belt. Geol. Bull. China 27, 1744–1751 (in Chinese with English Abstract).

Gao, L.Z., Dai, C.G., Liu, Y.X., Wang, M., Wang, X.H., Chen, J.S., Ding, X.Z., 2010. Zircon SHRIMP U-Pb dating of the tuffaceous bed of Xiajiang Group in Guizhou Province and its stratigraphic implication. Geol. China 37, 1071–1080 (in Chinese with English Abstract).

Gao, L.Z., Chen, J., Ding, X.Z., Liu, Y.R., Zhang, C.H., Zhang, H., Liu, Y.X., Pang, W.H., Zhang, Y.H., 2011. Zircon SHRIMP U-Pb dating of the tuff bed of Lengjiaxi and Banxi groups, northeastern Hunan: constraints on the Wuling Movement. Geol. Bull. China 30, 1001–1008 (in Chinese with English Abstract).

Gao, L.Z., Liu, Y.X., Ding, X.Z., Song, Z.R., Huang, Z.Z., Zhang, C.H., Zhang, H., Shi, Z.G., 2013a. Geochronographic dating of the Tieshajie formation in the Jiangshan-Shaoxing fault zone and its implications. Geol. Bull. China 32, 996–1005 (in Chinese with English Abstract).

Gao, L.Z., Lu, J.P., Ding, X.Z., Wang, H.R., Liu, Y.X., Li, J., 2013b. Zircon U-Pb dating of Neoproterozoic tuff in South Guangxi and its implications for stratigraphic correlation. Geol. China 40, 1443–1452 (in Chinese with English Abstract).

Gao, L.Z., Zhang, H., Ding, X.Z., Liu, Y.X., Zhang, C.H., Huang, Z.Z., Xu, X.M., Zhou, Z.Y., 2014a. SHRIMP U-Pb dating of the Jianshan-Shaoxing faulted zone in Zhejiang and Jiangxi. Geol. Bull. China 33, 763–775 (in Chinese with English Abstract).

Gao, L.Z., Chen, J.S., Dai, C.G., Ding, X.Z., Wang, X.H., Liu, Y.X., Wang, M., Zhang, H., 2014b. SHRIMP zircon U-Pb dating of tuff in Fanjingshan Group and Xiajiang Group from Guizhou and Hunan Provinces and its stratigraphic implications. Geol. Bull. China 33, 949–959 (in Chinese with English Abstract).

Gao, L.Z., Yin, C.Y., Ding, X.Z., Wang, Z.J., Zhang, H., 2015. Rating data of the Neoproterozoic chronostratigraphy and stratigraphic correlation in South China. Acta Geoscientica Sinica 36, 533–545 (in Chinese with English Abstract).

Griffin, W.L., Pearson, N.J., Belousova, E.A., Jackson, S.E.E.V.A., O'Reilly, S.Y., Shee, S. R., 2000. The Hf isotope composition of cratonic mantle: LAM-MC-ICPMS analysis of zircon megacrysts in kimberlites. Geochim. Cosmochim. Acta 64, 133–147.

Griffin, W.L., Wang, X., Jackson, S.E., Pearson, N.J., O'Reilly, S.Y., Xu, X.-S., Zhou, X.-M., 2002. Zircon chemistry and magma mixing, SE China: in-situ analysis of Hf isotopes, Tonglu and Pingtan igneous complexes. Lithos 61, 237–269.

Hacker, B.R., Ratschbacher, L., Webb, L., McWilliams, M.O., Ireland, T., Calvert, A., Dong, S., Wenk, H.R., Chateigner, D., 2000. Exhumation of ultrahigh-pressure continental crust in east central China: late Triassic-Early Jurassic tectonic unroofing. J. Geophys. Res.: Solid Earth 105, 13339–13364.

Han, Y.G., Zhao, G.C., Cawood, P.A., Sun, M., Eizenhöfer, P.R., Hou, W.Z., Zhang, X.R., Liu, Q., 2016. Tarim and North China cratons linked to northern Gondwana through switching accretionary tectonics and collisional orogenesis. Geology 44, 95–98.

Harris, N.B.W., Pearce, J.A., Tindle, A.G., 1986. Geochemical characteristics of collision-zone magmatism. In: Coward, M.P., Ries, A.C. (Eds.), Collision Tectonics, vol. 19. Geol. Soc. Spec. Publ., pp. 67–81.

Harrison, T.M., Watson, E.B., Aikman, A.B., 2007. Temperature spectra of zircon crystallization in plutonic rocks. Geology 35, 635.

He, H.L., Li, B., Han, L.R., Sun, D.Z., Wang, S.X., Li, S., 2002. Evaluation of determining 47 elements in geological samples by pressurized acid digestion-ICPMS. Chin. J. Anal. Lab. 21, 8–12 (in Chinese with English Abstract).

Huang, X.L., Xu, Y.G., Li, X.H., Li, W.X., Lan, J.B., Zhang, H.H., Liu, Y.S., Wang, Y.B., Li, H. Y., Luo, Z.Y., Yang, Q.J., 2008. Petrogenesis and tectonic implications of Neoproterozoic, highly fractionated A-type granites from Mianning, South China. Precambr. Res. 165, 190–204.

Keay, S., Steele, D., Compston, W., 1999. Identifying granite sources by SHRIMP U-Pb zircon geochronology: an application to the Lachlan fold belt. Contrib. Mineral. Petrol. 137, 323–341.

Li, H.K., Zhu, S.X., Xiang, Z.Q., Su, W.B., Lu, S.N., Zhou, H.Y., Li, S., Yang, F.J., 2010. Zircon U-Pb dating on tuff bed from Gaoyuzhuang Formation in Yanqing, Beijing: further constraints on the new subdivision of the Mesoproterozoic stratigraphy in the northern North China Craton. Acta Petrol. Sin. 26, 2131–2140 (in Chinese with English Abstract).

Li, J.H., Zhang, Y.Q., Dong, S.W., Su, J.B., Li, Y., Cui, J.J., Shi, W., 2013. The Hengshan low-angle normal fault zone: structural and geochronological constraints on the Late Mesozoic crustal extension in South China. Tectonophysics 606, 97–115.

Li, J.H., Zhang, Y.Q., Dong, S.W., Johnston, S.T., 2014. Cretaceous tectonic evolution of South China: a preliminary synthesis. Earth Sci. Rev. 134, 98–136.

Li, J.H., Shi, W., Zhang, Y.Q., Dong, S.W., Ma, Z.L., 2016a. Thermal evolution of the Hengshan extensional dome in central South China and its tectonic implications: new insights into low-angle detachment formation. Gondwana Res. 35, 425–441.

Li, L.M., Lin, S.F., Xing, G.F., Davis, D.W., Jiang, Y., Davis, W., Zhang, Y.J., 2016b. Ca. 830 Ma back-arc type volcanic rocks in the eastern part of the Jiangnan Orogen: implications for the Neoproterozoic tectonic evolution of South China Block. Precambr. Res. 275, 209–224.

Li, J.H., Dong, S.W., Zhang, Y.Q., Zhao, G.C., Johnston, S.T., Cui, J.J., Xin, Y.J., 2016c. New insights into Phanerozoic tectonics of south China: Part 1, polyphase deformation in the Jiuling and Lianyunshan domains of the central Jiangnan Orogen. J. Geophys. Res.: Solid Earth 121, 3048–3080.

Li, L.M., Sun, M., Wang, Y.J., Xing, G.F., Zhao, G.C., He, Y.H., He, K.J., Zhang, A.M., 2011. U-Pb and Hf isotopic study of detrital zircons from the meta-sedimentary rocks in central Jiangxi Province, South China: implications for the Neoproterozoic tectonic evolution of South China Block. J. Asian Earth Sci. 41, 44–55.

Li, L.M., Lin, S.F., Xing, G.F., Davis, D.W., Davis, W.J., Xiao, W.J., Yin, C.Q., 2013a. Geochemistry and tectonic implications of late Mesoproterozoic alkaline bimodal volcanic rocks from the Tieshajie Group in the southeastern Yangtze Block, South China. Precambr. Res. 230, 179–192.

Li, L.M., Lin, S.F., Xing, G.F., Davis, D.W., Davis, W.J., Xiao, W.J., Yin, C.Q., 2013b. Geochronology and geochemistry of volcanic rocks from the Shaojiwa Formation and Xingzi Group, Lushan area, SE China: Implications for Neoproterozoic back-arc basin in the Yangtze Block. Precambr. Res. 238, 1–17.

Li, W.X., Li, X.H., 2003. Adakitic granites within the NE Jiangxi ophiolites, South China: geochemical and Nd isotopic evidence. Precambr. Res. 122, 29–44.

Li, W.X., Li, X.H., Li, Z.X., 2005. Neoproterozoic bimodal magmatism in the Cathaysia Block of South China and its tectonic significance. Precambr. Res. 136, 51–66.

Li, W.X., Li, X.H., Li, Z.X., Lou, F.S., 2008. Obduction-type granites within the NE Jiangxi Ophiolite: Implications for the final amalgamation between the Yangtze and Cathaysia Blocks. Gondwana Res. 13, 288–301.

Li, X.H., Zhou, G.Q., Zhao, J.X., Fanning, C.M., Compston, W., 1994. SHRIMP ion microprobe zircon U-Pb age and Sm-Nd isotopic characteristics of the NE Jiangxi ophiolite and its tectonic implications. Chin. J. Geochem. 13, 317–325 (in Chinese with English Abstract).

Li, X.H., Li, Z.X., Zhou, H.W., Liu, Y., Kinny, P.D., 2002b. U-Pb zircon geochronology, geochemistry and Nd isotopic study of Neoproterozoci bimodal volcanic rocks in the Kangdian Rift of South China: implications for the initial rifting of Rodinia. Precambr. Res. 113, 135–154.

Li, X.H., Li, Z.X., Ge, W.C., Zhou, H.W., Li, W.X., Liu, Y., Wingate, M.T.D., 2003a. Neoproterozoic granitoids in South China: crustal melting above a mantle plume at ca. 825 Ma? Precambr. Res. 122, 45–83.

Li, X.H., Li, W.X., Li, Z.X., Liu, Y., 2008c. 850–790 Ma bimodal volcanic and intrusive rocks in northern Zhejiang, South China: a major episode of continental rift magmatism during the breakup of Rodinia. Lithos 102, 341–357.

Li, X.H., Li, W.X., Li, Z.X., Lo, C.H., Wang, J., Ye, M.F., Yang, Y.H., 2009. Amalgamation between the Yangtze and Cathaysia Blocks in South China: constraints from SHRIMP U-Pb zircon ages, geochemistry and Nd-Hf isotopes of the Shuangxiwu volcanic rocks. Precambr. Res. 174, 117–128.

Li, Z.X., Zhang, L.H., Powell, C.M., 1995. South China in Rodinia: part of the missing link between Australia-East Antarctica and Laurentia? Geology 23, 407.

Li, Z.X., Li, X.H., Kinny, P.D., Wang, J., 1999. The breakup of Rodinia: did it start with a mantle plume beneath South China? Earth Planet. Sci. Lett. 173, 171–181.

Li, Z.X., Li, X.H., Zhou, H.W., Kinny, P.D., 2002a. Grenvillian continental collision in south China: new SHRIMP U-Pb zircon results and implications for the configuration of Rodinia. Geology 30, 163.

Li, Z.X., Li, X.H., Kinny, P.D., Wang, J., Zhang, S., Zhou, H., 2003b. Geochronology of Neoproterozoic syn-rift magmatism in the Yangtze Craton, South China and correlations with other continents: evidence for a mantle superplume that broke up Rodinia. Precambr. Res. 122, 85–109.

Li, Z.X., Wartho, J.A., Occhipinti, S., Zhang, C.L., Li, X.H., Wang, J., Bao, C.M., 2007. Early history of the eastern Sibao Orogen (South China) during the assembly of Rodinia: New mica $^{40}Ar/^{39}Ar$ dating and SHRIMP U-Pb detrital zircon provenance constraints. Precambr. Res. 159, 79–94.

Liu, Y.S., Hu, Z.C., Gao, S., Günther, D., Xu, J., Gao, C.G., Chen, H.H., 2008. In situ analysis of major and trace elements of anhydrous minerals by LA-ICP-MS without applying an internal standard. Chem. Geol. 257, 34–43.

Liu, Y.S., Gao, S., Hu, Z.C., Gao, C.G., Zong, K.D., Wang, D.B., 2010a. Continental and oceanic crust recycling-induced melt-peridotite interactions in the Trans-North China Orogen: U-Pb dating, Hf isotopes and trace elements in zircons from mantle xenoliths. J. Petrol. 51, 537–571.

Ludwig, K.R., 2003. User's Manual for Isoplot 3.00: A Geochronological Toolkit for Microsoft Excel, 4. Berkeley Geochronological Center Special Publication, pp. 71.

Maas, R., Nicholls, I.A., Legg, C., 1997. Igneous and metamorphic enclaves in the S-type Deddick Granodiorite, Lachlan Fold Belt, SE Australia: Petrographic, geochemical and Nd-Sr isotopic evidence for crustal melting and magma mixing. J. Petrol. 38, 815–841.

Mckenzie, D.P., Bickle, M.J., 1988. The volume and composition of melt generated by extension of the lithosphere. J. Petrol. 29, 625–679.

Middemost, E.A.K., 1994. Naming materials in the magma/igneous rock system. Earth Sci. Rev. 37, 215–224.

Miller, C.F., McDowell, S.M., Mapes, R.W., 2003. Hot and cold granites? Implications of zircon saturation temperatures and preservation of inheritance. Geology 31, 529.

Miniar, P.D., Piccoli, P.M., 1989. Tectonic discrimination of granitoids. Geol. Soc. Am. Bull. 101, 635–643.

Patino-Douce, A.E., Harris, A.N., 1998. Experimental constraints on Himalayan anatexis. J. Petrol. 39, 689–710.

Pearce, J.A., Harris, N.B.W., Tindle, A.G., 1984. Trace element discrimination diagrams for the tectonic interpretation of granitic rocks. J. Petrol. 25, 956–983.

Pearce, J.A., 1996. Sources and settings of granitic rocks. Episodes 19, 120–125.

Scherer, E., Münker, C., Mezger, K., 2001. Calibration of the lutetium-hafnium clock. Science 293.

Schmid, S.M., Fügenschuh, B., Kissling, E., Schuster, R., 2004. Tectonic map and overall architecture of the Alpine orogen. Swiss J. Geosci. 97, 93–117.

Shi, H.C., Shi, X.B., Yang, X.Q., Jiang, H.Y., 2013. The exhumation process of Mufushan granite in Jiangnan uplift since Cenozoic: evidence from low temperatures thermochronology. Chin. J. Geophys. 56, 1945–1957 (in Chinese with English Abstract).

Shu, L.S., Zhou, W.Q., Shi, Y.S., Yin, J., 1993. Study of high pressure metamorphicblueschist and its late Proterozoic age in the eastern Jiangnan belt. Chin. Sci. Bull. 38, 1879–1882 (in Chinese with English Abstract).

Shu, L.S., Shi, Y.S., Guo, L.Z., Charvet, J., Sun, Y., 1995. Plate Tectonic Evolution and the Kinematics of Collisional Orogeny in the Middle Jiangnan, Eastern China. Nanjing University Publication, pp. 174 (in Chinese with English Abstract).

Shu, L.S., Charvet, J., 1996. Kinematics and geochronology of the Proterozoic Dongxiang-Shexian ductile shear zone: with HP metamorphism and ophiolitic melange (Jiangnan Region, South China). Tectonophysics 267, 291–302.

Shu, L.S., Fature, M., Jiang, S.Y., Yang, Q., Wang, Y.J., 2006. SHRIMP zircon U-Pb age, litho- and biostratigraphic analyses of the Huaiyu Domain in South China. Episodes 29, 244–252.

Shu, L.S., Faure, M., Yu, J.H., Jahn, B.M., 2011. Geochronological and geochemical features of the Cathaysia block (South China): New evidence for the Neoproterozoic breakup of Rodinia. Precambr. Res. 187, 263–276.

Smithies, R.H., Champion, D.C., 2000. The Archaen high-Mg diorite suite: Links to tonalite-trondhjemite-granodiorite magmatism and implications for early Archaean crustal growth. J. Petrol. 41, 1653–1671.

Sun, S.S., McDonough, W.F., 1989. Chemical and isotopic systematics of oceanic basalt: implications for mantle composition and processes. In: Saunders, A.D., Norry, M.J. (Eds.), Magmatism in the Ocean Basins, 42. Geol. Soc. Spec. Publ., pp. 528–548.

Sylvester, P.J., 1998. Post-collisional strongly peraluminous granites. Lithos 45, 29–44.

Taylor, S.R., McLennan, S.M., 1985. The Continental Crust: Its Composition and Evolution. Oxford Press Blackwel, Washington, DC, pp. 1–312.
Taylor, S.R., McLennan, M.S., 1995. The geochemical evolution of the continental crust. Rev. Geophys. 33, 293–301.
Tommasi, A., Vauchez, A., 2001. Continental rifting parallel to ancient collisional belts: an effect of the mechanical anisotropy of the lithospheric mantle. Earth Planet. Sci. Lett. 185, 199–210.
Valley, J.W., Chiarenzelli, J.R., McLelland, J.M., 1994. Oxygen isotope geochemistry of zircon. Earth Planet. Sci. Lett. 126, 187–206.
Valley, J.W., 2003. Oxygen isotope in zircon. In: Hanchar, J.M., Hoskin, P.W.O. (Eds.), Zircon rev Mineral Geochem, vol 53. Mineral Soc Am, Washington, pp. 343–385.
Vauchez, A., Barruol, G., Tommasi, A., 1997. Why do continents break-up parallel to ancient orogenic belts? Terra Nova 9, 62–66.
Vervoort, J.D., Patchett, P.J., Soderlund, U., Baker, M., 2004. Isotopic composition of Yb and the determination of Lu concentrations and Lu/Hf ratios by isotope dilution using MC-ICPMS. Geochem. Geophys. Geosyst. 5, 325–348.
Villaros, A., Stevens, G., Moyen, J.F., Buick, I.S., 2009. The trace element compositions of S-type granites: evidence for disequilibrium melting and accessory phase entrainment in the source. Contrib. Miner. Petrol. 158, 543–561.
Wan, Y.S., Liu, D.Y., Wilde, S.A., Cao, J.J., Chen, B., Dong, C.Y., Song, B., Du, L.L., 2010. Evolution of the Yunkai Terrane, South China: evidence from SHRIMP zircon U-Pb dating, geochemistry and Nd isotope. J. Asian Earth Sci. 37, 140–153.
Wang, J., 2003. Zircon SHRIMP U-Pb dating for the Cangshuipu volcanic rocks and its implications for the lower boundary age of the Nanhua strata in South China. Chin. Sci. Bull. 48, 1663.
Wang, J., Li, Z.X., 2003. History of Neoproterozoic rift basins in South China: implications for Rodinia break-up. Precambr. Res. 122, 141–158.
Wang, L.X., Ma, C.Q., Zhang, C., Zhang, J.Y., Marks, M.A.W., 2014c. Genesis of leucogranite by prolonged fractional crystallization: a case study of the Mufushan complex, South China. Lithos 206–207, 147–163.
Wang, Q., Wyman, D.A., Li, Z.X., Bao, Z.W., Zhao, Z.H., Wang, Y.X., Jian, P., Yang, Y.H., Chen, L.L., 2010b. Petrology, geochronology and geochemistry of ca. 780 Ma A-type granites in South China: petrogenesis and implications for crustal growth during the breakup of the supercontinent Rodinia. Precambr. Res. 178, 185–208.
Wang, X.L., Zhou, J.C., Qiu, J.S., Gao, J.F., et al., 2004a. Comment on "Neoproterozoic granitoids in South China: crustal melting above a mantle plume at ca. 825 Ma?" by Xian-Hua Li, Precambrian Res. 122 (2003) 45–83. Precambr. Res. 132, 401–403.
Wang, X.L., Zhou, J.C., Qiu, J.S., Gao, J.F., 2004b. Geochemistry of the Meso- to Neoproterozoic basic–acid rocks from Hunan Province, South China: implications for the evolution of the western Jiangnan Orogen. Precambr. Res. 135, 79–103.
Wang, X.L., Zhou, J.C., Qiu, J.S., Zhang, W.L., Liu, X.M., Zhang, G.L., 2006a. LA-ICP-MS U-Pb zircon geochronology of the Neoproterozoic igneous rocks from Northern Guangxi, South China: implications for tectonic evolution. Precambr. Res. 145, 111–130.
Wang, X.L., Zhou, J.C., Griffin, W.L., Wang, R.C., Qiu, J.S., O'Reilly, S.Y., Xu, X.S., Liu, X. M., Zhang, G.L., 2007a. Detrital zircon geochronology of Precambrian basement sequences in the Jiangnan Orogen: Dating the assembly of the Yangtze and Cathaysia Blocks. Precambr. Res. 159, 117–131.
Wang, X.L., Zhao, G.C., Zhou, J.C., Liu, Y.S., Hu, J., 2008a. Geochronology and Hf isotopes of zircon from volcanic rocks of the Shuangqiaoshan Group, South China: implications for the Neoproterozoic tectonic evolution of the eastern Jiangnan Orogen. Gondwana Res. 14, 355–367.
Wang, X.L., Zhou, J.C., Qiu, J.S., Jiang, S.Y., Shi, Y.R., 2008b. Geochronology and geochemistry of Neoproterozoic mafic rocks from western Hunan, South China: implications for petrogenesis and post-orogenic extension. Geol. Mag. 145.
Wang, X.L., Shu, L.S., Xing, G.F., Zhou, J.C., Tang, M., Shu, X.J., Qi, L., Hu, Y.H., 2012a. Post-orogenic extension in the eastern part of the Jiangnan Orogen: evidence from ca 800–760 Ma volcanic rocks. Precambr. Res. 222–223, 404–423.
Wang, X.L., Zhou, J.C., Wan, Y.S., Kitajima, K., Wang, D., Bonamici, C., Qiu, J.S., Sun, T., 2013b. Magmatic evolution and crustal recycling for Neoproterozoic strongly peraluminous granitoids from southern China: Hf and O isotopes in zircon. Earth Planet. Sci. Lett. 366, 71–82.
Wang, X.L., Zhou, J.C., Griffin, W.L., Zhao, G., Yu, J.H., Qiu, J.S., Zhang, Y.J., Xing, G.F., 2014b. Geochemical zonation across a Neoproterozoic orogenic belt: isotopic evidence from granitoids and metasedimentary rocks of the Jiangnan Orogen, China. Precambr. Res. 242, 154–171.
Wang, X.S., Gao, J., Klemd, R., Jiang, T., Zhai, Q.G., Xiao, X.C., Liang, X.Q., 2015. Early Neoproterozoic multiple arc–back-arc system formation during subduction–accretion processes between the Yangtze and Cathaysia blocks: new constraints from the supra-subduction zone NE Jiangxi ophiolite (South China). Lithos 236–237, 90–105.
Wang, Y.J., Fan, W.M., Sun, M., Liang, X.Q., Zhang, Y.H., Peng, T.P., 2007b. Geochronological, geochemical and geothermal constraints on petrogenesis of the Indosinian peraluminous granites in the South China Block: a case study in the Hunan Province. Lithos 96, 475–502.
Wang, Y.J., Wu, C.M., Zhang, A.M., Fan, W.M., Zhang, Y.H., Zhang, Y.Z., Peng, T.P., Yin, C.Q., 2012c. Kwangsian and Indosinian reworking of the eastern South China Block: constraints on zircon U-Pb geochronology and metamorphism of amphibolites and granulites. Lithos 150, 227–242.
Wang, Y.J., Zhang, A.M., Cawood, P.A., Fan, W.M., Xu, J.F., Zhang, G.W., Zhang, Y.Z., 2013a. Geochronological, geochemical and Nd–Hf–Os isotopic fingerprinting of an early Neoproterozoic arc–back-arc system in South China and its accretionary assembly along the margin of Rodinia. Precambr. Res. 231, 343–371.
Wang, Y.J., Zhang, Y.Z., Fan, W.M., Geng, H.Y., Zou, H.P., Bi, X.W., 2014a. Early Neoproterozoic accretionary assemblage in the Cathaysia Block: geochronological, Lu–Hf isotopic and geochemical evidence from granitoid gneisses. Precambr. Res. 249, 144–161.
Wang, W., Wang, F., Chen, F.K., Zhu, X.Y., Xiao, P., Siebel, W., 2010a. Detrital zircon ages and Hf-Nd isotopic composition of Neoproterozoic sedimentary rocks in the Yangtze Block: constraints on the deposition age and provenance. J. Geol. 118, 79–94.
Wang, W., Zhou, M.F., 2012. Sedimentary records of the Yangtze Block (South China) and their correlation with equivalent Neoproterozoic sequences on adjacent continents. Sed. Geol. 265–266, 126–142.
Wang, W., Zhou, M.F., Yan, D.P., Li, J.W., 2012b. Depositional age, provenance, and tectonic setting of the Neoproterozoic Sibao Group, southeastern Yangtze Block, South China. Precambr. Res. 192–195, 107–124.
Wang, W., Zhou, M.F., 2013. Petrological and geochemical constraints on Provenance, paleoweathering, and tectonic setting of the Neoproterozoic sedimentary basin in the Eastern Jiangnan Orogen, South China. J. Sediment. Res. 83, 974–993.
Wang, W., Zhou, M.F., Yan, D.P., Li, L., Malpas, J., 2013c. Detrital zircon record of Neoproterozoic active-margin sedimentation in the eastern Jiangnan Orogen, South China. Precambr. Res. 235, 1–19.
Wang, W., Zhou, M.F., Zhao, J.H., Pandit, M.K., Zheng, J.P., Liu, Z.R., 2016. Neoproterozoic active continental margin in the southeastern Yangtze Block of South China: evidence from the ca. 830–810 Ma sedimentary strata. Sed. Geol. 342, 254–267.
White, A.J.R., Chappell, B.W., 1977. Ultrametamorphism and granitoid genesis. Tectonophysics 43, 7–22.
Wu, F.Y., Li, X.H., Zheng, Y.F., Gao, S., 2007. Lu-Hf isotopic systematics and their applications in petrology. Acta Petrol. Sin. 23, 185–220 (in Chinese with English Abstract).
Wu, R.X., Zheng, Y.F., Wu, Y.B., Zhao, Z.F., Zhang, S.B., Liu, X.M., Wu, F.Y., 2006. Reworking of juvenile crust: element and isotope evidence from Neoproterozoic granodiorite in South China. Precambr. Res. 146, 179–212.
Xia, Y., Xu, X.S., Zhao, G.C., Liu, L., 2015. Neoproterozoic active continental margin of the Cathaysia block: evidence from geochronology, geochemistry, and Nd–Hf isotopes of igneous complexes. Precambr. Res. 269, 195–216.
Xiao, W.J., Windley, B.F., Hao, J., Zhai, M.G., 2003. Accretion leading to collision and the Permian Solonker suture, Inner Mongolia, China: termination of the central Asian orogenic belt. Tectonics 22, 1–20.
Xiao, W.J., Kusky, T., Safonova, I., Seltmann, R., Sun, M., 2015. Tectonics of the Central Asian Orogenic Belt and its Pacific analogues. J. Asian Earth Sci. 113, 1–6.
Xu, X.B., Xue, D.J., Li, Y., Hu, P., Chen, N.S., 2014. Neoproterozoic sequences along the Dexing-Huangshan fault zone in the eastern Jiangnan Orogen, South China: geochronological and geochemical constrains. Gondwana Res. 25, 368–382.
Xue, H.M., Ma, F., Song, Y.Q., Xie, Y.P., 2010. Geochronology and geochemisty of the Neoproterozoic granitoid association from eastern segment of the Jiangnan Orogen, China: Constraints on the timing and process of amalgamation between the Yangtze and Cathaysia blocks. Acta Geol. Sin. 26, 3215–3244 (in Chinese with English Abstract).
Yang, C., Li, X.H., Wang, X.C., Lan, Z.W., 2015. Mid-Neoproterozoic angular unconformity in the Yangtze Block revisited: insights from detrital zircon U-Pb age and Hf–O isotopes. Precambr. Res. 266, 165–178.
Yao, J.L., Shu, L.S., Santosh, M., Li, J.Y., 2012. Precambrian crustal evolution of the South China Block and its relation to supercontinent history: constraints from U-Pb ages, Lu–Hf isotopes and REE geochemistry of zircons from sandstones and granodiorite. Precambr. Res. 208–211, 19–48.
Yao, J.L., Shu, L.S., Santosh, M., 2014a. Neoproterozoic arc-trench system and breakup of the South China Craton: constraints from N-MORB type and arc-related mafic rocks, and anorogenic granite in the Jiangnan Orogenic belt. Precambr. Res. 247, 187–207.
Yao, J.L., Shu, L.S., Santosh, M., Zhao, G.C., 2014b. Neoproterozoic arc-related mafic-ultramafic rocks and syn-collision granite from the western segment of the Jiangnan Orogen, South China: constraints on the Neoproterozoic assembly of the Yangtze and Cathaysia Blocks. Precambr. Res. 243, 39–62.
Yao, J.L., Shu, L.S., Santosh, M., Li, J.Y., 2015. Neoproterozoic arc-related andesite and orogeny-related unconformity in the eastern Jiangnan Orogenic belt: constraints on the assembly of the Yangtze and Cathaysia blocks in South China. Precambr. Res. 262, 84–100.
Yao, J.L., Cawood, P.A., Shu, L.S., Santosh, M., Li, J.Y., 2016a. An early Neoproterozoic accretionary prism ophiolitic mélange from the western Jiangnan Orogenic Belt, South China. J. Geol. 125, 587–601.
Yao, J.L., Shu, L.S., Cawood, P.A., Li, J.Y., 2016b. Delineating and characterizing the boundary of the Cathaysia Block and the Jiangnan orogenic belt in South China. Precambr. Res. 275, 265–277.
Ye, M.F., Li, X.H., Li, W.X., Liu, Y., Li, Z.X., 2007. SHRIMP zircon U-Pb geochronological and whole-rock geochemical evidence for an early Neoproterozoic Sibaoan magmatic arc along the southeastern margin of the Yangtze Block. Gondwana Res. 12, 144–156.
Yin, A., Harrison, T.M., 2000. Geologic evolution of the Himalayan-Tibetan orogen. Annu. Rev. Earth Planet. Sci. 28, 211–280.
Yin, C.Q., Lin, S.F., Davis, D.W., Xing, G.F., Davis, W.J., Cheng, G.H., Xiao, W.J., Li, L.M., 2013. Tectonic evolution of the southeastern margin of the Yangtze Block: constraints from SHRIMP U-Pb and LA-ICP-MS Hf isotopic studies of zircon from the eastern Jiangnan Orogenic Belt and implications for the tectonic interpretation of South China. Precambr. Res. 236, 145–156.

Zhang, A.M., Wang, Y.J., Fan, W.M., Zhang, Y.Z., Yang, J., 2012c. Earliest Neoproterozoic (ca. 1.0 Ga) arc-back-arc basin nature along the northern Yunkai Domain of the Cathaysia Block: geochronological and geochemical evidence from the metabasite. Precambr. Res. 220–221, 217–233.
Zhang, C.L., Zou, H.B., Zhu, Q.B., Chen, X.Y., 2015. Late Mesoproterozoic to early Neoproterozoic ridge subduction along southern margin of the Jiangnan Orogen New evidence from the Northeastern Jiangxi Ophiolite (NJO), South China. Precambr. Res. 268, 1–15.
Zhang, H., Li, T.D., Gao, L.Z., Geng, S.F., Ding, X.Z., Liu, Y.X., Kou, C.H., 2015a. Zircon SHRIMP dating, geochemical, zircon Hf isotopic features of the Mesoproterozoic Tieshajie Formation in northerneastern Jiangxi. Geol. Rev. 61, 65–78 (in Chinese with English Abstract).
Zhang, Q.R., Li, X.H., Feng, L.J., Huang, J., Song, B., 2008a. A new age constraint on the onset of the Neoproterozoic glaciations in the Yangtze Platform, South China. J. Geol. 116, 423–429.
Zhang, S.B., Wu, R.X., Zheng, Y.F., 2012b. Neoproterozoic continental accretion in South China: geochemical evidence from the Fuchuan ophiolite in the Jiangnan Orogen. Precambr. Res. 220–221, 45–64.
Zhang, S.H., Jiang, G.Q., Dong, J., Han, Y.G., Wu, H.C., 2008b. New SHRIMP U-Pb age from the Wuqiangxi Formation of Banxi Group: implications for rifting and stratigraphic erosion associated with the early Cryogenian (Sturtian) glaciation in South China. Sci. China Series D 38, 1496–1503 (in Chinese with English Abstract).
Zhang, Y.Z., Wang, Y.J., Fan, W.M., Zhang, A.M., Ma, L.Y., 2012a. Geochronological and geochemical constraints on the metasomatised source for the Neoproterozoic (~825 Ma) high-Mg volcanic rocks from the Cangshuipu area (Hunan Province) along the Jiangnan domain and their tectonic implications. Precambr. Res. 220–221, 139–157.
Zhang, Y.Z., Wang, Y.J., Geng, H.Y., Zhang, Y.H., Fan, W.M., Zhong, H., 2013. Early Neoproterozoic (~850 Ma) back-arc basin in the Central Jiangnan Orogen (Eastern South China): geochronological and petrogenetic constraints from meta-basalts. Precambr. Res. 231, 325–342.
Zhang, Y.Z., Wang, Y.J., Zhang, Y.H., Zhang, A.M., 2015b. Neoproterozoic assembly of the Yangtze and Cathaysia blocks: evidence from the Cangshuipu Group and associated rocks along the Central Jiangnan Orogen, South China. Precambr. Res. 269, 18–30.
Zhang, Y.Z., Wang, Y.J., 2016. Early Neoproterozoic (~840 Ma) arc magmatism: geochronological and geochemical constraints on the metabasites in the Central Jiangnan Orogen. Precambr. Res. 275, 1–17.
Zhao, G.C., Cawood, P.A., 1999. Tectonothermal evolution of the Mayuan assemblage in the Cathaysia block: implications for Neoproterozoic collision-related assembly of the South China craton. Am. J. Sci. 299, 309–339.
Zhao, G.C., Cawood, P.A., 2012. Precambrian geology of China. Precambr. Res. 222–223, 13–54.
Zhao, G.C., 2015. Jiangnan Orogen in South China: developing from divergent double subduction. Gondwana Res. 27, 1173–1180.
Zhao, J.H., Zhou, M.F., 2007a. Geochemistry of Neoproterozoic mafic intrusions in the Panzhihua district (Sichuan Province, SW China): implications for subduction-related metasomatism in the upper mantle. Precambr. Res. 152, 27–47.
Zhao, J.H., Zhou, M.F., 2007b. Neoproterozoic adakitic plutons and arc magmatism along the western margin of the Yangtze Block, South China. J. Geol. 115, 675–689.
Zhao, J.H., Zhou, M.F., Yan, D.P., Yang, Y.H., Sun, M., 2008. Zircon Lu–Hf isotopic constraints on Neoproterozoic subduction-related crustal growth along the western margin of the Yangtze Block, South China. Precambr. Res. 163, 189–209.
Zhao, J.H., Zhou, M.F., Zheng, J.P., Fang, S.M., 2010. Neoproterozoic crustal growth and reworking of the Northwestern Yangtze Block: constraints from the Xixiang dioritic intrusion, South China. Lithos 120, 439–452.
Zhao, J.H., Zhou, M.F., Yan, D.P., Zheng, J.P., Li, J.W., 2011. Reappraisal of the ages of Neoproterozoic strata in South China: no connection with the Grenvillian orogeny. Geology 39, 299–302.
Zhao, J.H., Zhou, M.F., Zheng, J.P., 2013. Constraints from zircon U-Pb ages, O and Hf isotopic compositions on the origin of Neoproterozoic peraluminous granitoids from the Jiangnan Fold Belt, South China. Contrib. Miner. Petrol. 166, 1505–1519.
Zheng, Y.F., Zhang, S.B., Zhao, Z.F., Wu, Y.B., Li, X.H., Li, Z.X., Wu, F.Y., 2007. Contrasting zircon Hf and O isotopes in the two episodes of Neoproterozoic granitoids in South China: implications for growth and reworking of continental crust. Lithos 96, 127–150.
Zheng, Y.F., Wu, R.X., Wu, Y.B., Zhang, S.B., Yuan, H.L., Wu, F.Y., 2008. Rift melting of juvenile arc-derived crust: Geochemical evidence from Neoproterozoic volcanic and granitic rocks in the Jiangnan Orogen, South China. Precambr. Res. 163, 351–383.
Zhong, Y.F., Ma, C.Q., She, Z.B., Lin, G.C., Xu, H.J., Wang, R.J., Yang, K.G., Liu, Q., 2005. SHRIMP U-Pb zircon geochronology of the Jiuling granitic complex batholith in Jiangxi Province. Earth Science – J. China Univ. Geosci. 30. 685-591 (in Chinese with English Abstract).
Zhou, J.C., Wang, X.L., Qiu, J.S., Gao, J.F., 2004. Geochemistry of Meso- and Neoproterozoic mafic-ultramafic rocks from northern Guangxi, China: arc or plume magmatism. Geochem. J. 38, 139–152.
Zhou, J.C., Wang, X.L., Qiu, J.S., 2009. Geochronology of Neoproterozoic mafic rocks and sandstones from northeastern Guizhou, South China: coeval arc magmatism and sedimentation. Precambr. Res. 170, 27–42.
Zhou, M.F., Yan, D.P., Kennedy, A.K., Li, Y.Q., Ding, J., 2002a. SHRIMP U-Pb zircon geochronological and geochemical evidence for Neoproterozoic arc-magmatism along the western margin of the Yangtze Block, South China. Earth Planet. Sci. Lett. 196, 51–67.
Zhou, M.F., Kennedy, A.K., Sun, M., Malpas, J., Lesher, C.M., 2002b. Neoproterozoic arc-related mafic intrusions along the northern margin of South China: implications for the accretion of Rodinia. J. Geol. 110, 611–618.
Zhou, M.F., Ma, Y.X., Yan, D.P., Xia, X.P., Zhao, J.H., Sun, M., 2006a. The Yanbian Terrane (Southern Sichuan Province, SW China): a Neoproterozoic arc assemblage in the western margin of the Yangtze Block. Precambr. Res. 144, 19–38.
Zhou, M.F., Yan, D.P., Wang, C.L., Qi, L., Kennedy, A., 2006b. Subduction-related origin of the 750 Ma Xuelongbao adakitic complex (Sichuan Province, China): implications for the tectonic setting of the giant Neoproterozoic magmatic event in South China. Earth Planet. Sci. Lett. 248, 286–300.
Zhou, X.H., Zhang, Y.J., Liao, S.B., Yu, M.G., Chen, Z.H., Zhao, X.L., Jiang, Y., Jiang, R., 2012. LA-ICP-MS zircon U-Pb geochronology of volcanic rocks in the Shuangqiaoshan Group at Anhui-Jiangxi Boundary region and its geological implication. Geol. J. China Univ. 18, 609–622 (in Chinese with English Abstract).